© 2021. Published by The Company of Biologists Ltd | Development (2021) 148, dev192674. doi:10.1242/dev.192674

RESEARCH ARTICLE

Roles of developmentally regulated KIF2A alternative isoforms in cortical neuron migration and differentiation

Cansu Akkaya[1], Dila Atak[1,*], Altug Kamacioglu[1], Busra Aytul Akarlar[1], Gokhan Guner[1,‡], Efil Bayam[1,§], Ali Cihan Taskin[2], Nurhan Ozlu[1] and Gulayse Ince-Dunn[1,3,¶]

ABSTRACT

KIF2A is a kinesin motor protein with essential roles in neural progenitor division and axonal pruning during brain development. However, how different KIF2A alternative isoforms function during development of the cerebral cortex is not known. Here, we focus on three *Kif2a* isoforms expressed in the developing cortex. We show that *Kif2a* is essential for dendritic arborization in mice and that the functions of all three isoforms are sufficient for this process. Interestingly, only two of the isoforms can sustain radial migration of cortical neurons; a third isoform, lacking a key N-terminal region, is ineffective. By proximity-based interactome mapping for individual isoforms, we identify previously known KIF2A interactors, proteins localized to the mitotic spindle poles and, unexpectedly, also translation factors, ribonucleoproteins and proteins that are targeted to organelles, prominently to the mitochondria. In addition, we show that a KIF2A mutation, which causes brain malformations in humans, has extensive changes to its proximity-based interactome, with depletion of mitochondrial proteins identified in the wild-type KIF2A interactome. Our data raises new insights about the importance of alternative splice variants during brain development.

KEY WORDS: Alternative splicing, KIF2A, Cortical development, Proximity-interactome mapping

INTRODUCTION

Alternative splicing (AS) is one of the major molecular processes underlying increased transcriptome and proteome diversity and associated organismal complexity in metazoans (Dhananjaya et al., 2018; Su et al., 2018; Zhang et al., 2016; Zhang et al., 2014). High-throughput sequencing efforts have revealed that approximately 95% of all genes in the human body are alternatively spliced, generating more than 100,000 different mRNA isoforms, and the vast majority of isoform functions are completely unknown. AS is especially prevalent in the nervous system (Pan et al., 2008; Wang et al., 2008) and its impairment is often associated with neurological disease (Irimia et al., 2014; Scotti and Swanson, 2016). AS is dynamically regulated during brain development, where it modulates important processes including neural progenitor cell-to-neuron transition, migration, axon guidance and synaptogenesis (Raj and Blencowe, 2015; Su et al., 2018; Yeo et al., 2004). Despite important advances in our understanding of how AS is regulated in a tissue-specific manner to allow transcriptome and proteome diversification, little is known about how individual alternative isoforms function to regulate nervous system development. In particular, only a small fraction of neurodevelopmental studies have investigated functions of distinct isoforms, and only the most abundant isoform is typically studied. Here, we have focused on the separable functions of three different isoforms of the kinesin motor protein 2A (KIF2A) within the context of mouse cerebral cortex development.

KIF2A, a microtubule (MT)-depolymerizing kinesin, functions in mitotic spindle assembly (Ganem and Compton, 2004) and primary cilium disassembly in mitotic cells (Miyamoto et al., 2015; Zhang et al., 2019), and in axonal pruning in differentiating neurons (Homma et al., 2018; Maor-Nof et al., 2013). In humans, mutations in the motor domain of KIF2A are causative for malformations of cortical development, manifesting as lissencephaly, microcephaly, pachygyria and heterotopias (Broix et al., 2018; Cavallin et al., 2017; Poirier et al., 2013; Tian et al., 2016). Recent studies have suggested that *Kif2a* AS is regulated by neuron-specific RNA-binding proteins (Ince-Dunn et al., 2012) and its isoform abundance dynamically shifts during the neural progenitor-to-neuron transition during development of the cerebral cortex (Zhang et al., 2016). However, how individual KIF2A isoforms function during cortical development has not been studied previously. Here, we show that KIF2A is essential for proper dendritic arborization of cortical neurons and that all three KIF2A isoforms are interchangeable during this process. Moreover, we demonstrate that only two of the three KIF2A isoforms can functionally support radial neuronal migration in mice. We reveal isoform-specific interacting protein partners of KIF2A by a proximity-ligation-based proteomic study carried out in a neuronal cell line. In addition to a number of MT-binding proteins, our interactome screen also identifies mitochondrial proteins and nuclear RNA-binding proteins as either common or isoform-specific interactors, raising a potential role for KIF2A in mitochondrial assembly and RNA localization. Finally, we apply our proximity-based interactome mapping approach using KIF2A^{H321D}, which harbors a dominant-negative point mutation causative for malformations of cortical development in humans (Broix et al., 2018; Poirier et al., 2013). Intriguingly, we find significant rewiring of the protein interactome of KIF2A^{H321D}, with a remarkable loss of interactions with almost all mitochondrial proteins identified in wild-type KIF2A. Our results highlight the importance of investigating isoform-specific functions of gene products regulated by AS and reveal the utility of proximity based interactome mapping in identifying separable roles for either protein isoforms or mutants.

[1]Department of Molecular Biology and Genetics, Koç University, 34450 Istanbul, Turkey. [2]Embryo Manipulation Laboratory, Animal Research Facility, Translational Medicine Research Center, Koç University, 34450 Istanbul, Turkey. [3]Stem Cells and Metabolism Research Program, Faculty of Medicine, University of Helsinki, 00290 Helsinki, Finland.
*Present address: Translational Medicine Research Center, Koç University, 34450 Istanbul, Turkey. ‡Present address: German Center for Neurodegenerative Diseases (DZNE), Munich 81377, Germany. §Present address: Institute of Genetics and Molecular and Cellular Biology (IGBMC), Inserm U964, CNRS UMR7104, University of Strasbourg, 67404 Illkirch, France.

¶Author for correspondence (gulayse.dunn@helsinki.fi)

C.A., 0000-0001-7911-1755; G.G., 0000-0002-5875-5815; N.O., 0000-0002-5157-8780; G.I.-D., 0000-0003-1352-990X

Handling Editor: François Guillemot
Received 8 May 2020; Accepted 18 January 2021

Development (2021) 148, dev192674. doi:10.1242/dev.192674

RESULTS

Kif2a alternative isoform expression is developmentally regulated in mouse cerebral cortex

A previous study aimed at identifying the regulated targets of neuronal Elav-like RNA binding proteins (nElavl RNABPs) in the developing mouse cortex had identified *Kif2a* pre-mRNA as a top target (Ince-Dunn et al., 2012). In mice, the *Kif2a* gene consists of 20 coding exons, and nElavl proteins promote the inclusion of exon 18, which encodes for 37 amino acids rich in serine residues. While cloning these two major isoforms from the postnatal mouse cerebral cortex, we also identified a third isoform that includes exon 18, along with a shorter (by 20 amino acids) exon 5 generated as a result of alternative 5′ splice site selection (Fig. 1A). We numbered these isoforms as *Kif2a.1* (exon 18+ and long exon 5), *Kif2a.2* (exon 18− and long exon 5) and *Kif2a.3* (exon 18+ and short exon 5) (Fig. 1A).

Next, we quantified the relative mRNA abundance of the three *Kif2a* isoforms in the developing cerebral cortex using quantitative RT-PCR. Our results demonstrated that *Kif2a.1* and *Kif2a.2* were the predominant isoforms, manifesting higher embryonic expression levels compared with postnatal and adult stages. *Kif2a.3* was generally the minor isoform, with expression peaking during late embryogenesis and once again during the second postnatal week (Fig. 1B). Taken together, our results indicate an overall trend in which expression of *Kif2a* isoforms is high during embryonic and early postnatal stages of corticogenesis, a time period in which neural progenitor proliferation, active neuronal migration and dendritogenesis ensues.

KIF2A isoforms are interchangeable in their roles for dendritic arborization of cortical neurons

To understand whether the three KIF2A isoforms may have divergent functions we asked whether AS had an effect on their subcellular localization. For this purpose, we imaged all three KIF2A isoforms in Neuro2A cells and primary cortical neurons after expressing EGFP-KIF2A fusion proteins of individual isoforms. Our images revealed that all three KIF2A isoforms are localized predominantly to the cytoplasm and nucleus in both cell types (Fig. 2A; Fig. S1). Furthermore, all three isoforms similarly localized to the soma, axons, dendrites and growth cones in primary neurons (Fig. 2A; Fig. S2). Our results therefore suggest that AS of KIF2A does not influence its subcellular localization in Neuro2A cells and cultured cortical neurons.

Previous studies have demonstrated a role for KIF2A in pruning of axon collaterals of cortical neurons and sensory neurons in mice (Homma et al., 2003; Maor-Nof et al., 2013). As regulation of MT dynamics is also crucial for dendritic arbor growth and pruning (Urbanska et al., 2008), we next evaluated the role of KIF2A isoforms in dendrite development. Initially, we verified that KIF2A was indeed expressed specifically in neurons and not in glia of our primary cultures, by carrying out co-immunofluorescent stainings against KIF2A and the neuronal marker NEUROD2 or the glial marker GFAP (Fig. S3). Next, we knocked down *Kif2a* expression in primary cortical neurons by expressing a short hairpin RNA (shRNA) targeting a common sequence in all three isoforms (Fig. 2B). We co-expressed soluble EGFP for imaging neuronal processes and measured dendritic arborization by Sholl analysis, which is a quantitative measure of dendritic length and branching (Fig. 2D) (Ferreira et al., 2014; Schindelin et al., 2012). Our results revealed a significant increase in the number of primary dendrites, consistent with a diminished capacity for MT depolymerization and dendritic pruning in the absence of KIF2A (Fig. 2E). In order to test the ability of different KIF2A isoforms to carry out their role in dendrite arborization, we knocked down all *Kif2a* expression, and then returned one isoform at a time by re-introducing shRNA-resistant forms of individual isoforms (*resKif2a.1*, *resKif2a.2* and *resKif2a.3*) (Fig. 2C,D). As above, we quantified dendritic development by Sholl analysis. Our analysis revealed that all three isoforms of KIF2A were able to suppress the growth of superfluous dendrite branches and could reverse the KIF2A loss-of-function phenotype equally well (Fig. 2F-H). Taken together, we conclude that KIF2A is required for normal dendrite development in

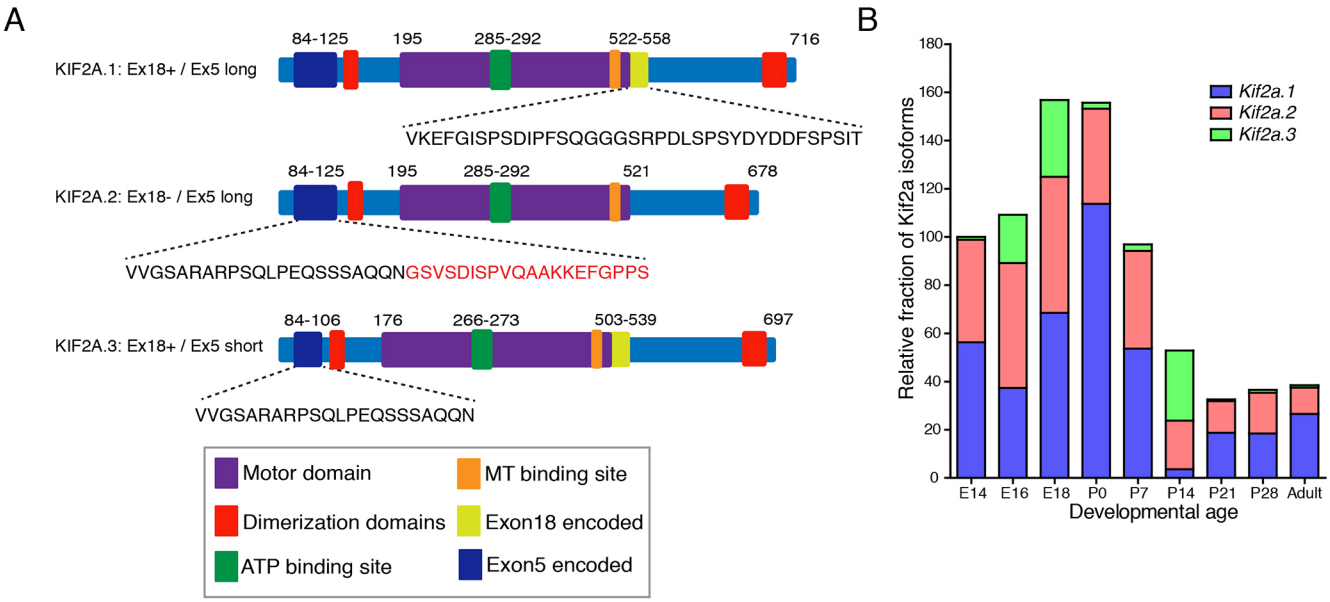

Fig. 1. KIF2A expression is developmentally controlled in mouse cortex. (A) Schematic of three different KIF2A isoforms shown as KIF2A.1, KIF2A.2 and KIF2A.3. Amino acid sequences of exon 18, exon 5-long and exon 5-short are indicated, and the amino acid sequence absent in exon 5 of KIF2A.3 is highlighted in red. (B) The relative fraction of *Kif2a* isoform expression (normalized to first *Gapdh* and then to the levels measured in E14 tissue) quantified by qRT-PCR analysis. Data represent three biological and two technical replicates.

Development (2021) 148, dev192674. doi:10.1242/dev.192674

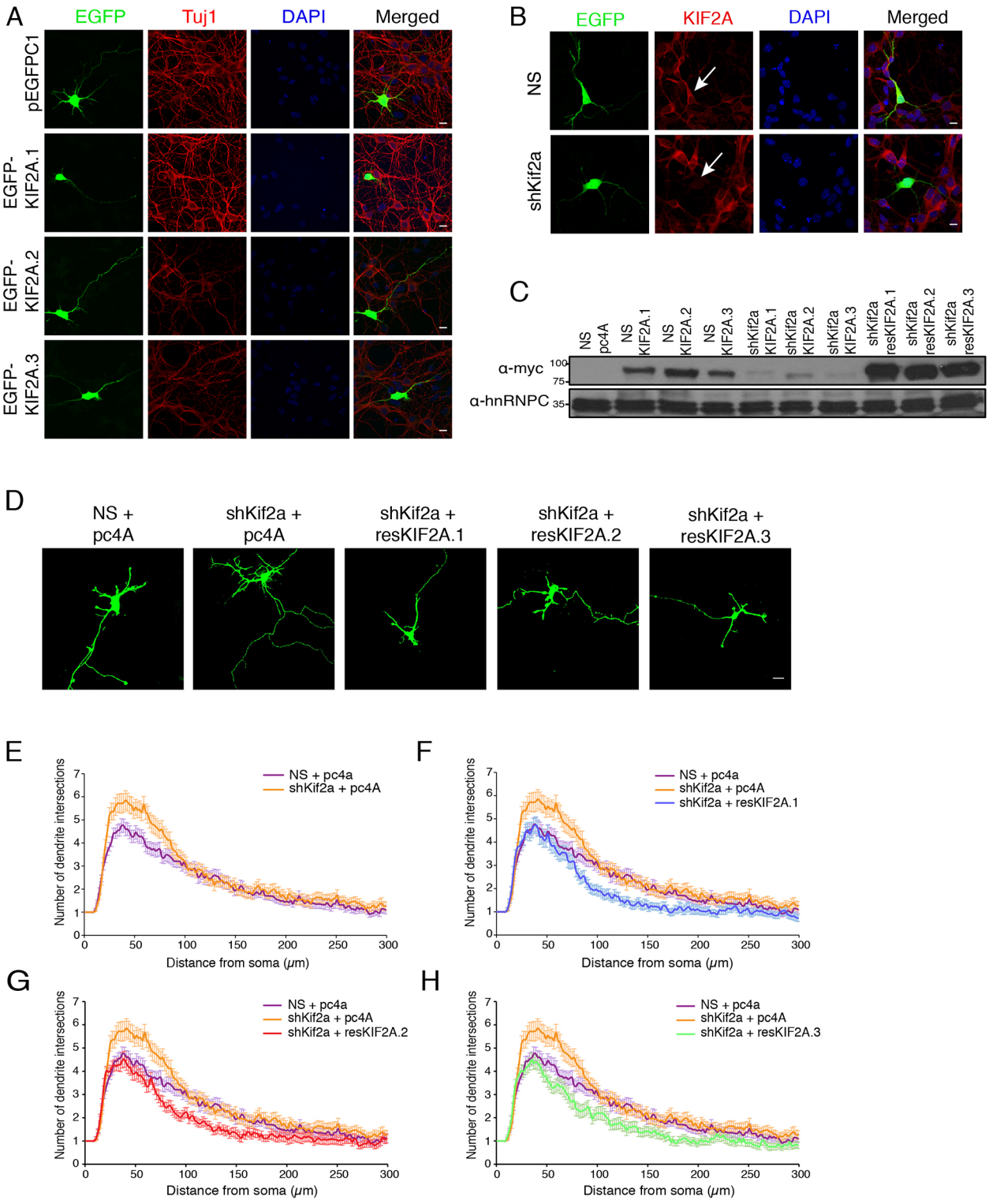

Fig. 2. KIF2A isoforms function in dendritic arborization. (A) Primary cortical neurons from E18.5 embryos transfected with plasmids expressing pEGFPC1-KIF2A (KIF2A.1, KIF2A.2 and KIF2A.3 separately) at 2 days *in vitro* (DIV), fixed and immunostained with anti-GFP at 4 DIV. Microtubules were visualized with anti-Tuj1 antibody (red). (B) E14.5 primary cortical neurons were transfected with EGFP-tagged non-silencing shRNA (NS) or EGFP-tagged shRNA against KIF2A (*shKif2a*) at 2 DIV, fixed at 4 DIV and immunostained against EGFP (green) and KIF2A (red) proteins. Transfected cells were identified based on their co-expression of EGFP from NS or shRNA-expressing plasmid. White arrows indicate transfected neurons. (C) Immunoblotting against myc-tagged *Kif2a* isoforms, expression of which is suppressed by co-expression of *shKif2a*. The *resKif2a* cDNAs are resistant to silencing by *shKif2a*. hnRNPC is used as a loading control. (D) Representative images of primary cortical neurons from E14.5 embryos co-transfected with NS or *shKif2a* along with either the pcDNA4A (pc4A) backbone or *resKif2a* isoforms at 2 DIV, fixed at 4 DIV and imaged with confocal microscopy. (E-H) Dendrite arborization was quantified by Sholl analysis for NS, *shKif2a* (E), NS, *shKif2a*, *resKif2a.1* (F), NS, *shKif2a*, *resKif2a.2* (G) and NS, *shKif2a*, *resKif2a.3* (H). *n*=60 for each condition derived from two separate neuronal cultures. Bars represent s.e.m. $P<0.0001$ by two-way ANOVA (E). The plots for NS and *shKif2a* samples are replicated in E,F,G and H for ease of comparison of *shKif2a* and samples expressing shRNA-resistant *Kif2a* isoforms. Scale bars: 10 µm.

Development (2021) 148, dev192674. doi:10.1242/dev.192674

cortical neurons and all three KIF2A isoforms may carry out this function.

Specific KIF2A isoforms appear to play a role in radial migration of cortical neurons

Previous studies have demonstrated that KIF2A is required for cortical neuronal migration (Broix et al., 2018; Ding et al., 2019). Mutations in *Kif2a* affect neuronal positioning in the cerebral cortex and cause cortical malformations in humans (Broix et al., 2018; Ding et al., 2019; Poirier et al., 2013). Consequently, we investigated whether the role of KIF2A in cortical neuronal migration is isoform-dependent. During development, the neural progenitor cells divide in the ventricular zone (VZ) of the embryonic telencephalon. After exiting the cell cycle, the early neurons radially migrate through the subventricular and intermediate zones (SVZ-IZ) until they reach the most superficial layer of the developing cortical plate (CP) (Kriegstein and Noctor, 2004). In order to assess the role of different KIF2A isoforms in this process, we knocked down expression of all *Kif2a* isoforms, then re-introduced one isoform at a time by expressing shRNA-resistant *Kif2a* cDNAs in ventricular neural progenitors of embryonic day (E) 14.5 cerebral cortex by *in utero* electroporation. We also electroporated a plasmid expressing the tdTomato marker and quantified the extent of neuronal migration by quantifying the number of tdTomato-positive neurons as a function of distance away from the VZ (Fig. 3A,B). As expected, in control samples ∼45% of tdTomato-positive neurons had reached the CP, ∼50% were migrating along the SVZ-IZ region and ∼5% were localized to the VZ at 3 days post-electroporation (Fig. 3A). Consistent with previous observations (Broix et al., 2018; Ding et al., 2019), there was a dramatic reduction in the relative fraction of tdTomato-positive neurons localized to the CP in *Kif2a* knockdown samples, and deficient migration caused most of the neurons to accumulate in the SVZ-IZ (Fig. 3A). In cortices where *Kif2a* expression was rescued with either *resKif2a.1* or *resKif2a.2*, neurons could exit the SVZ-IZ and reach the CP, at levels comparable with control samples (Fig. 3C,D,F,G). In contrast, *resKif2a.3*-expressing neurons exhibited a severe migration defect, and the number of neurons that could migrate to the cortical plate was significantly reduced (Fig. 3E,H). It is noteworthy to mention that KIF2A.3 differs from the other two isoforms by 20 amino acids encoded by exon 5, which corresponds to a disordered protein region predicted by the IUPred2A prediction tool (Dosztányi, 2018) (Fig. S4). Interestingly, tissue-specific splicing of disordered protein regions is increasingly acknowledged as a means to increase interaction networks across tissue (Buljan et al., 2013). Taken together, our results suggest that KIF2A.1 and KIF2A.2 isoforms, but not the KIF2A.3 isoform, can support neuronal migration in the developing cortex.

Proximity-labeling proteomics analysis of KIF2A isoforms reveal novel isoform-specific interactors

Experimental analysis and computational modeling have suggested that an important function of AS is to increase phenotypic complexity by expanding the interactome (Buljan et al., 2013; Ellis et al., 2012; Kandoi and Dickerson, 2019). Therefore, we next asked whether different KIF2A isoforms were indeed characterized by different protein interaction networks. Toward this goal, we performed a proximity-labeling method which allows the identification of potential interactors of a protein of interest by its expression as a promiscuous biotin-ligase (the *BirA** gene) fusion in the cell type of choice, followed by streptavidin-based affinity purification and mass spectrometry analysis (BioID) (Roux et al., 2013). In order to harvest sufficient total biotinylated protein, we decided to use the easily transfectable Neuro2A neuronal cell line for our BioID experiments. Initially, we confirmed that our BirA*-KIF2A fusion proteins were functional. For this, we transiently transfected BirA*-KIF2A fusions for each of the three isoforms, supplemented the cells with 0.05 mM biotin and 1 mM ATP, and confirmed that biotinylated proteins did indeed co-localize with expressed BirA*-KIF2A fusion proteins (Fig. 4A). Next, we verified that biotinylation was dependent upon the external supply of biotin, and that the background signal in the absence of external biotin following streptavidin pulldown was very low (Fig. 4B,C).

Having validated the BioID approach, we scaled up our protocol and deployed tandem mass spectrometry for analysis of purified proteins after streptavidin pulldown. We analyzed three biological replicates for each isoform, and based on peptide spectra match (PSM) values, we filtered out proteins identified in only one of the replicates, those with false discovery rate (FDR)>0.05, and those with fold-change<1.5. Non-transfected Neuro2A cells were used as control for background subtraction. Following these cut-off criteria, we identified a total of 63 potential interactors for KIF2A.1, 37 for KIF2A.2 and 40 for KIF2A.3 (Fig. 5A,G; Table S1). As expected, KIF2A itself was among the highest ranking hits for each of the three isoforms. We identified proteins that were common among all three KIF2A isoforms, shared in all possible pairwise combinations, as well as those that were unique for KIF2A.1, KIF2A.2 or KIF2A.3 (Fig. 5A,G; Table S1). Next we carried out gene ontology (GO) and interactome analysis using the String Database (Cline et al., 2007; Doncheva et al., 2019; Raudvere et al., 2019; Szklarczyk et al., 2019) separately with interactors of each of the KIF2A isoforms (Fig. 5D-F). As expected, a number of MT-associated proteins which function at the spindle poles during mitotic division were identified among the interactomes of at least one of the isoforms (e.g. CKAP5, NUMA1, CEP170 and MAP4). Our analysis revealed the highest number of interactors for KIF2A.1. Intriguingly, these were enriched for mitochondrial proteins with functions in mitochondrial gene expression (e.g. TIMM44, PNPT1, LARS2, RARS2 and TSFM) and metabolism (e.g. GLS, ALDH2, OAT, SUCLG2 and SUCLA2), and nuclear RNA regulation (e.g. SRSF3, SRSF4, SRRM2 and HNRNPA1) (Fig. 5D,G). KIF2A.2 displayed the least number of interactors, many of which were shared with KIF2A.1, with similar functions in mitochondrial metabolism and nuclear RNA transport (Fig. 5E,G). KIF2A.3 displayed the highest relative fraction of unique interactors. Its interactome was enriched in functions relating to nuclear RNA transport and regulation. Unlike the other two isoforms, KIF2A.3 was largely devoid of genes functioning in the mitochondria (Fig. 5F,G). Intriguingly, all KIF2A isoforms also appeared to interact with different eukaryotic translation factors (EIF5, EIF4G2, EEF1B2 and EIF3E). Finally, in order to verify that our BioID approach was able to identify endogenous interactions of KIF2A, we analyzed interaction between KIF2A and reticulon 4 (RTN4; also known as NOGO-A), which was identified in all three KIF2A isoform samples. Our co-immunofluorescence staining with KIF2A and RTN4 antibodies displayed a partial co-localization (Fig. S5). We also confirmed interaction by proximity ligation assay (PLA), which is a sensitive and specific method for detecting protein interactions with spatial resolution (Debaize et al., 2017). Our PLA results revealed a significant interaction between KIF2A and RTN4, compared with negative controls in which only anti-KIF2A or anti-RTN4 primary antibodies were used for the PLA protocol (Fig. 5B,C). In sum, our data identify common and unique interactors of the three KIF2A isoforms.

Development (2021) 148, dev192674. doi:10.1242/dev.192674

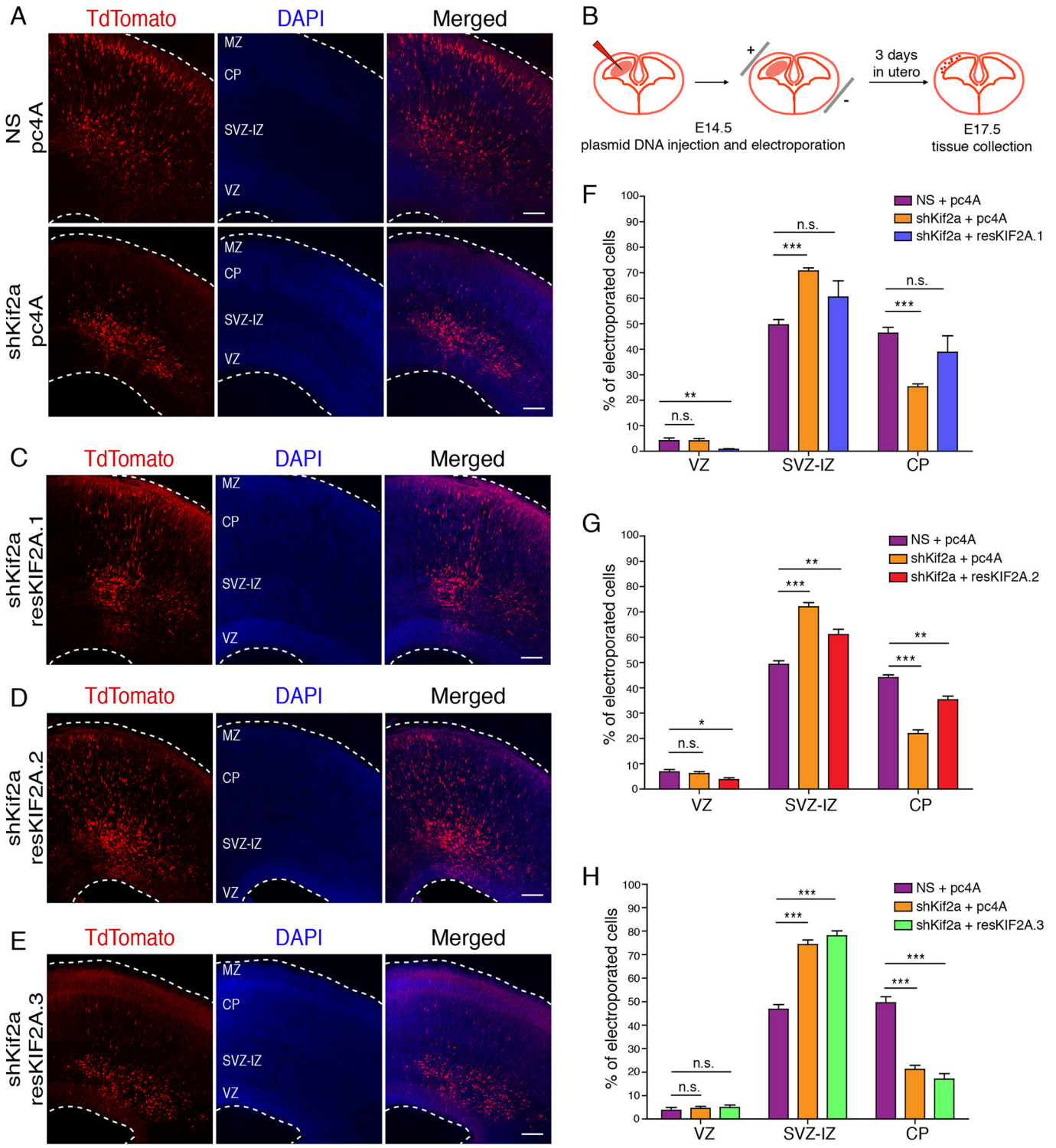

Fig. 3. Roles of different KIF2A isoforms in radial migration. (A) DAPI staining of E17.5 coronal sections *in utero* electroporated with either NS or *shKif2a* along with pcDNA4A (pc4A) and tdTomato at E14.5. (B) Relevant plasmid DNA expressing *shKif2a*, *resKif2a* and *tdTomato* were injected into the ventricle of E14.5 mice. Following a brief pulse of electroporation, embryos were replaced back into the uterus and allowed to develop for 3 days *in utero*. At E17.5 the embryonic cortices were collected for migration analysis. (C-E) Embryos electroporated *in utero* with *shKif2a* along with one of the *resKif2a.1* (C), *resKif2a.2* (D) or *resKif2a.3* (E) and tdTomato at E14.5. Boundaries of cortical sections are indicated as white dashed lines. (F-H) Quantification of *in utero* electroporation experiment of *resKif2a.1* (F), *resKif2a.2* (G) and *resKif2a.3* (H). Cortical sections were divided into zones. Percentages of tdTomato-positive neurons counted in individual zones are plotted (KIF2A.1: a total of *n*=4017 for NS, *n*=4572 for *shKif2a*, *n*=2696 for *resKif2a.1* from three biological replicates; KIF2A.2: a total of *n*=2477 for NS, *n*=3160 for *shKif2a*, *n*=3558 for *resKif2a.2* from two biological replicates; KIF2A.3: a total of *n*=3189 for NS, *n*=4456 for *shKif2a*, *n*=3549 for *resKif2a.3* from three biological replicates). Data are mean±s.e.m. **P*<0.05, ***P*<0.005, ****P*<0.0001 (unpaired two-tailed *t*-test). n.s., non-significant. MZ, marginal zone; CP, cortical plate; SVZ-IZ, subventricular zone-intermediate zone; VZ, ventricular zone. Scale bars: 100 µm.

Development (2021) 148, dev192674. doi:10.1242/dev.192674

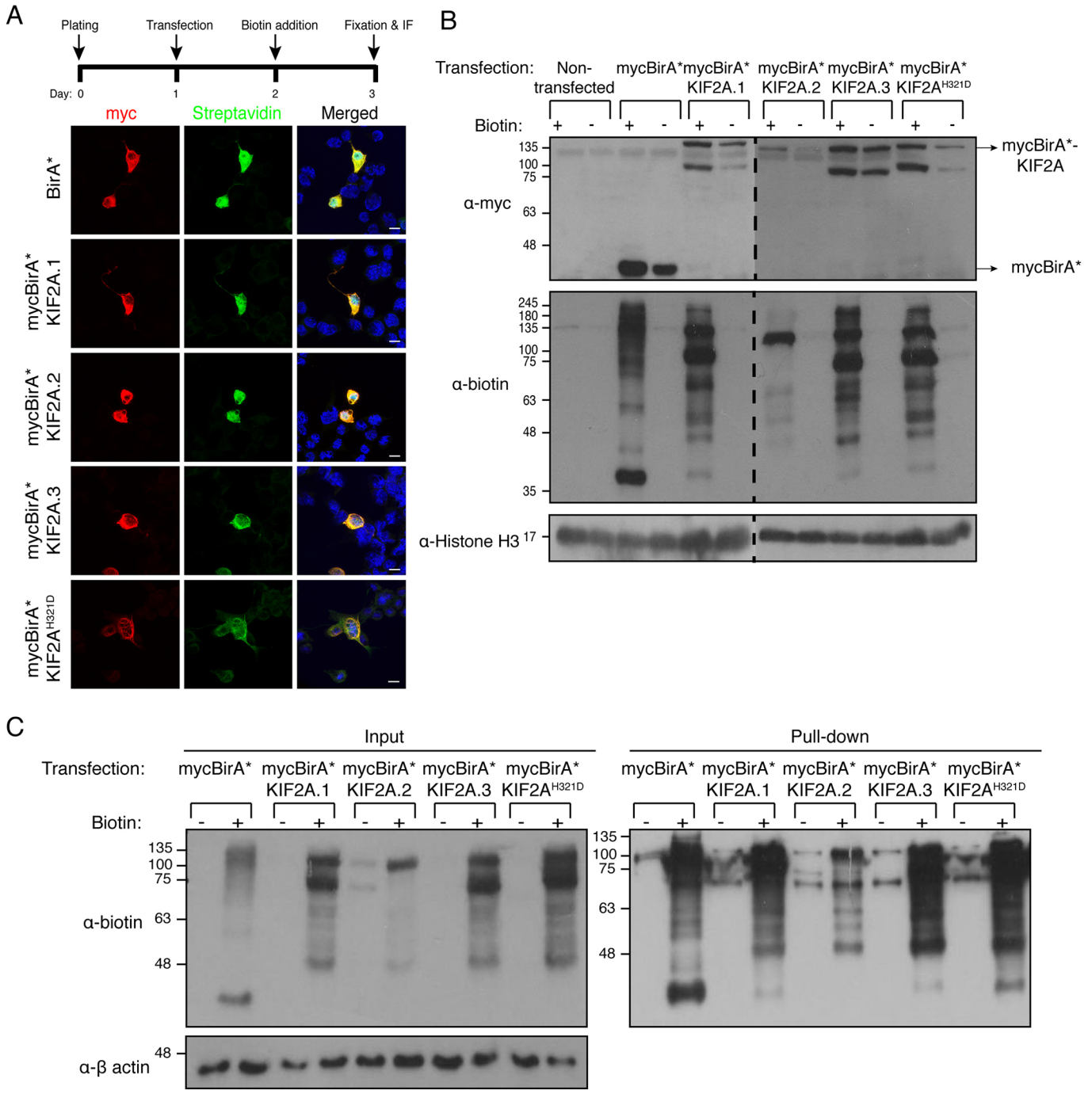

Fig. 4. Proximity biotin ligation assay of KIF2A isoforms in Neuro2A cells. (A) Immunofluorescence staining of myc (red), streptavidin (green) and DNA (blue) in Neuro2A cells transfected with *mycBirA**, *mycBirA*-Kif2a.1*, *mycBirA*-Kif2a.2*, *mycBirA*-Kif2a.3* or *mycBirA*-Kif2a^{H321D}* separately. Transfected cells were identified based on myc immunostaining. (B) Top panel: Immunoblotting with anti-myc showing expression of mycBirA*-KIF2A in Neuro2A cells. Middle panel: Immunoblotting with anti-biotin confirming biotinylation. Bottom panel: Anti-Histone H3 as loading control. (C) Pull-down with streptavidin beads followed by anti-biotin immunoblotting of Neuro2A cell lysates. Biotin supplementation to cell media is indicated. β-Actin is used as loading control for input blot. Scale bars: 10 µm.

KIF2A disease mutation causes rewiring of its protein interactome

Having established a system to uncover the protein interaction network of KIF2A, we next decided to turn our attention to KIF2A mutations that cause developmental cortical malformations in humans (KIF2A^{S317N} and KIF2A^{H321D}; Broix et al., 2018; Poirier et al., 2013). Initially, we generated identical disease-associated point mutations at conserved residues in the backbone of mouse *Kif2a.1* cDNA. To evaluate how these two KIF2A.1 mutants localize subcellularly in neuronal cells, we expressed EGFP-KIF2A^{S317N} and EGFP-KIF2A^{H321D} in Neuro2A cells and mouse primary cortical neurons. Consistent with previous observations (Broix et al., 2018; Poirier et al., 2013), both KIF2A^{S317N} and KIF2A^{H321D} mutants were sequestered along polymerized MTs and did not display the typical cytoplasmic and nuclear distribution pattern we observed for wild-type KIF2A.1 in both cell types (Figs 6A and 7B).

Development (2021) 148, dev192674. doi:10.1242/dev.192674

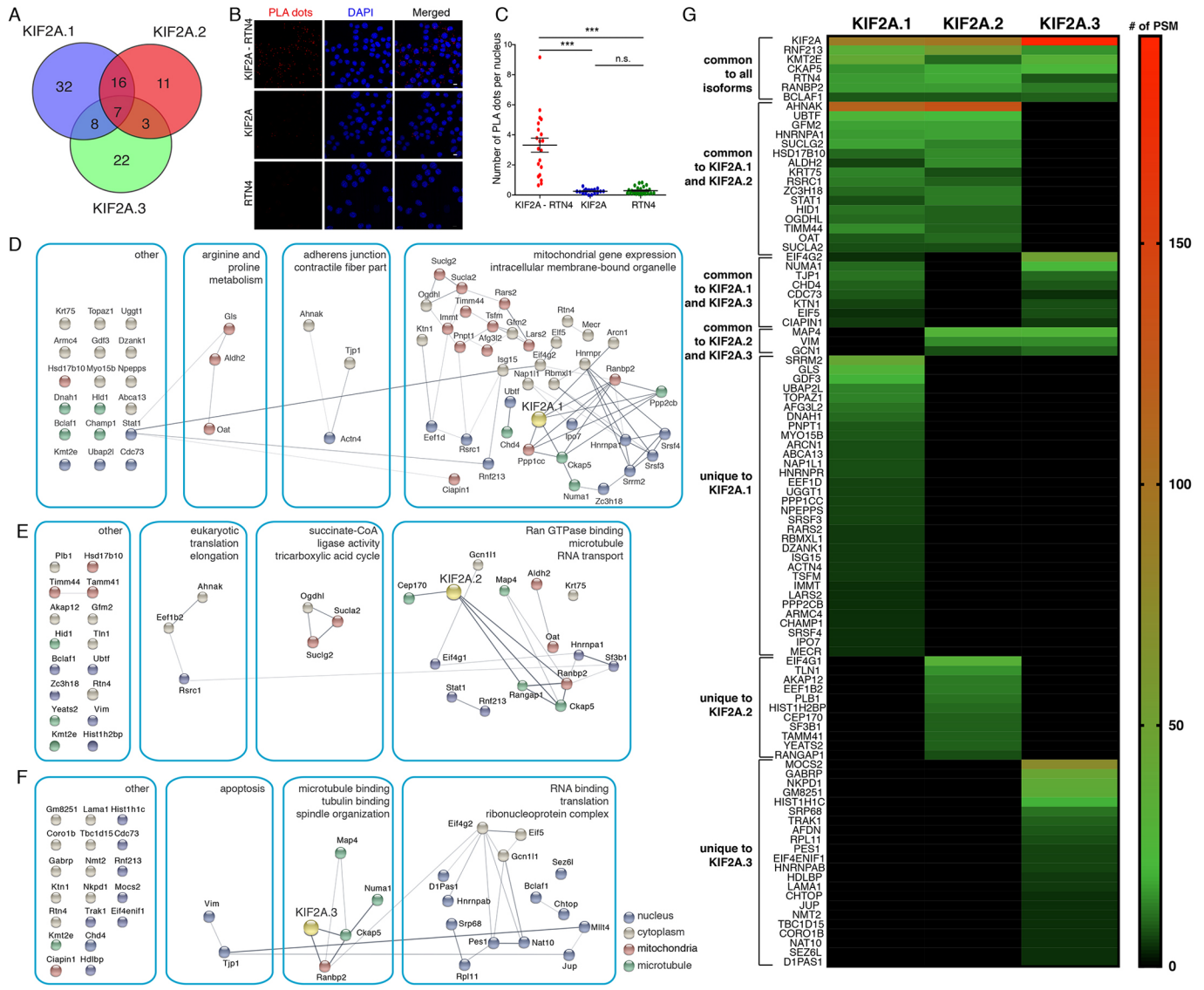

Fig. 5. Protein interactome of KIF2A isoforms is revealed by a proximity labeling proteomics. (A) Venn diagram represents the number of common and specific proximal protein partners of KIF2A isoforms. *n*=3 biological (two technical) replicates. (B) KIF2A interacts with RTN4 in a spatiotemporal resolution. Immunofluorescence staining of PLA dots (red), DNA (blue) in Neuro2A cells. (C) Spatial analysis of KIF2A-RTN4 interaction by PLA assay with 20 image frames (*n*=25 frames for RTN4) chosen randomly. Neuro2A cells fixed in 3.2% paraformaldehyde (PFA) were incubated with KIF2A-RTN4 antibody pairs (*n*=1052) for interaction analysis. Fixed cells incubated with only KIF2A (*n*=684) or only RTN4 (*n*=373) were used as control. Data are mean number of PLA dots per nucleus±s.e.m. ***P<0.0001 (one-way ANOVA with Bonferroni post hoc test). n.s., non-significant. (D-F) Interaction networks of significantly enriched proteins for KIF2A.1 (D), KIF2A.2 (E) and KIF2A.3 (F) are constructed by STRING database (Szklarczyk et al., 2019). Highly interconnected subnetworks are highlighted with blue rectangles and enriched GO and KEGG terms of each network are reported (Cline et al., 2007; Raudvere et al., 2019). The nodes with more than one annotated location are only illustrated with one compartment. Isoforms are indicated as yellow circles. Proteins are colored according to their localization in the cell: gray, cytoplasm; blue, nucleus; green, microtubule; red, mitochondria. Gray lines represent the known interactions from the STRING database and the thickness indicates an increase in interaction confidence. (G) Heat map generated through peptide spectra match values of proteins that were identified with BioID method for three KIF2A isoforms. Scale bars: 10 µm.

Next, we asked whether these dominant mutations affected dendrite development in cortical neurons. For this purpose, we co-transfected E14.5 mouse primary cortical neurons with a non-silencing shRNA or *shKif2a* along with either one of the shRNA-resistant *Kif2a* mutants (*resKif2a*^{S317N} or *resKif2a*^{H321D}) and carried out Sholl analysis. We confirmed that these mutations did not cause protein instability and were expressed at levels comparable with wild-type KIF2A (Fig. S6). We observed significantly increased dendrite arborization in neurons when *Kif2a* was silenced (Fig. 6B,C). Furthermore, co-expressing shRNA-resistant forms of either *Kif2a*^{S317N} or *Kif2a*^{H321D} did not rescue this defect, whereas wild-type *Kif2a.1* did so efficiently (Fig. 6B-F). Interestingly, if we expressed *Kif2a*^{S317N} or *Kif2a*^{H321D} in otherwise wild-type neurons without silencing endogenous *Kif2a*, we did not observe any effect on dendrite arborization (Fig. S7). Therefore, our results suggest that disease-causing dominant mutations in *Kif2a* cause dendrite arborization defects in primary cortical neurons, and this effect depends on the expression level of endogenous wild-type KIF2A.

Next, we analyzed results from our previous BioID proximity labeling experiments in which KIF2A^{H321D} (along with the three isoforms) was used as a bait. We compared proteins identified in

Development (2021) 148, dev192674. doi:10.1242/dev.192674

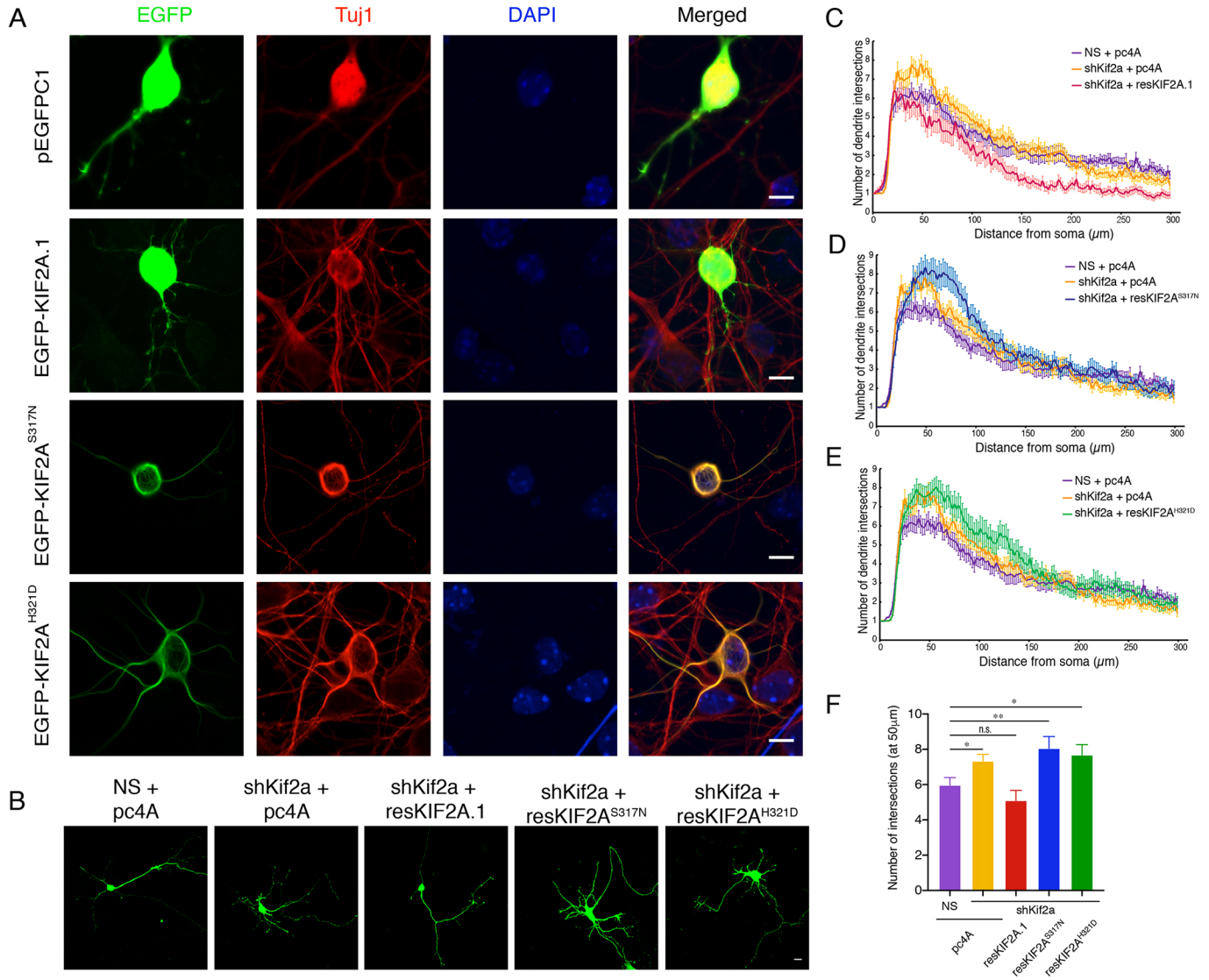

Fig. 6. *Kif2a* disease mutants cause dendrite development defects in primary cortical neurons. (A) E18.5 primary cortical neurons were transfected with plasmids expressing pEGFPC1-tagged KIF2A.1, KIF2A^{S317N} or KIF2A^{H321D} and immunostained with anti-GFP (green) and anti-Tuj1 (red). DNA was stained with DAPI. (B) Representative images of E14.5 primary cortical neurons from E14.5 embryos co-transfected with NS or *shKif2a* along with either pDNA4A backbone vector or shRNA-resistant wild-type *Kif2a* (*resKif2a.1*) or *Kif2a* mutants (*resKif2a*^{S317N} and *resKif2a*^{H321D}) at 2 DIV and fixed at 4 DIV. (C-E) Sholl analysis was performed to quantify dendrite arborization (Ferreira et al., 2014; Schindelin et al., 2012) on NS, *shKif2a*, *resKif2a.1* (C), NS, *shKif2a*, *resKif2a*^{S317N} (D) and NS, *shKif2a*, *resKif2a*^{H321D} (E). *n*=62 for NS, *n*=61 for *shKif2a*, *n*=47 for *resKif2a.1*, *n*=48 for *resKif2a*^{S317N} and *n*=49 for *resKif2a*^{H321D} derived from two separate neuronal cultures. The plots for NS and *shKif2a* samples are replicated in C,D and E for easy comparison with resKIF2A.1, resKIF2A^{S317N} and resKIF2A^{H321D}. (F) Quantification of number of dendrite intersections calculated by Sholl analysis at 50 µm distance from center of the neuronal soma. Data are mean±s.e.m. *P<0.05, **P<0.005 (unpaired two-tailed *t*-test). n.s., non-significant. Scale bars: 10 µm.

KIF2A^{H321D} and KIF2A.1 samples as the mutation was created within this isoform. Our comparison revealed widespread rewiring of the interactome upon introduction of the H321D mutation. We identified 52 proteins that were unique to KIF2A.1, 31 unique to KIF2A^{H321D} and 11 that were common to both (Fig. 4A-C; Fig. 7A,E; Table S1). Next, we generated a GO and interactome map for KIF2A^{H321D} and compared it to that of KIF2A.1, using the String database (Cline et al., 2007; Doncheva et al., 2019; Raudvere et al., 2019; Szklarczyk et al., 2019). The relative fraction of cytoplasmic, nuclear and MT-associated genes was preserved in KIF2A^{H321D}; however, the identities were different (Fig. 7C-E). The most striking observation was the depletion of mitochondrial proteins from the interactome of KIF2A^{H321D} in comparison with KIF2A.1 (16 mitochondrial proteins out of a total of 63 proteins for KIF2A.1 and one out of 42 for KIF2A^{H321D}).

KIF2A isoforms and disease mutants display different levels of co-localization with mitochondria

Our proximity biotinylation results from Neuro2A cells revealing a large number of unexpected potential interactions with mitochondrial proteins for isoforms KIF2A.1 and KIF2A.2, but far fewer for KIF2A.3 isoform and KIF2A^{H321D} mutant, prompted us to further analyze mitochondrial proximity of KIF2A in primary cortical neurons. We tested whether individual KIF2A isoforms and mutants displayed differential levels of co-localization with mitochondria by co-transfecting primary cortical neurons with EGFP-KIF2A fusion

Development (2021) 148, dev192674. doi:10.1242/dev.192674

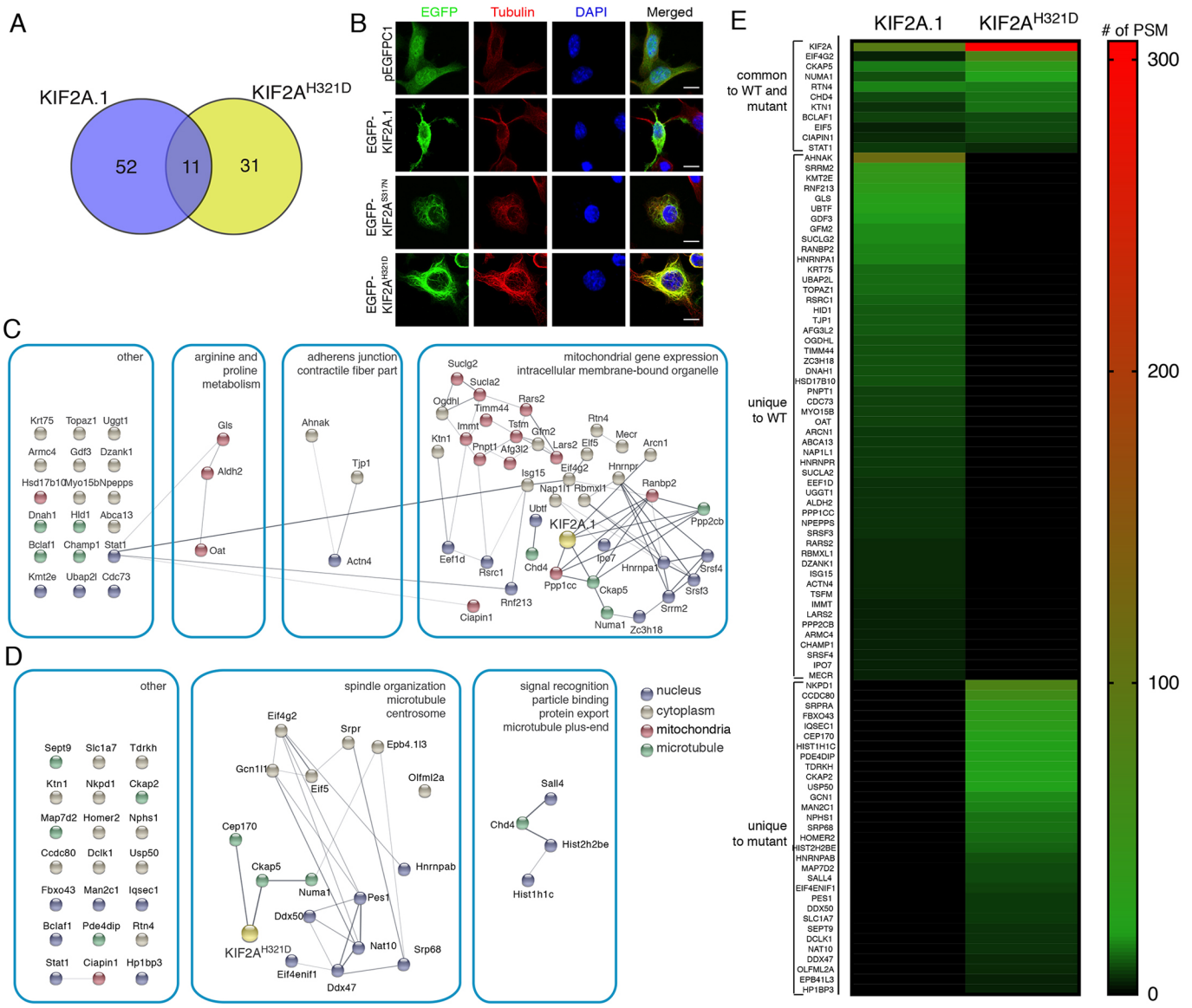

Fig. 7. Protein interactome of KIF2A^{H321D} is revealed by a proximity labeling proteomics. (A) Venn diagram representing the number of common and specific proximal protein partners of KIF2A.1 and KIF2A^{H321D}. *n*=3 biological (two technical) replicates. (B) Both KIF2A^{S317N} and KIF2A^{H321D} are co-localized predominantly to microtubules in Neuro2A cells. Neuro2A cells were transfected with plasmids expressing pEGFPC1-tagged KIF2A.1, KIF2A^{S317N} or KIF2A^{H321D} and immunostained with anti-GFP (green) or anti-α-tubulin (red) antibodies. (C,D) STRING interaction (Szklarczyk et al., 2019) network of candidate proteins identified for KIF2A.1 (C) and KIF2A^{H321D} (D) (Cline et al., 2007; Raudvere et al., 2019). Gray lines indicate known interactions and thickness represents confidence of interaction (see Fig. 5 for labeling). (E) Heat map created based on the peptide spectra match values of proteins that are identified with BioID of KIF2A.1 and KIF2A^{H321D}. Scale bars: 10 µm.

constructs together with mCherry fused to the outer mitochondrial protein TOMM20 (mCherry-TOMM20). Two days after transfection we imaged neurons by confocal microscopy and calculated Manders' co-localization coefficients for soma, axon and dendrite compartments (Fig. 8A,C). We used cytoplasmic EGFP-expressing neurons as negative controls. In the soma, KIF2A.1 and KIF2A.2 isoforms displayed levels of mitochondrial co-localization which were generally comparable with those of the negative controls, and KIF2A.3 showed a slight but statistically significant reduction (Fig. 8B; Fig. S8). Within the axon and dendrite compartments both KIF2A.1 and KIF2A.2 isoforms displayed significantly increased mitochondrial co-localization; however, this effect was less pronounced for KIF2A.3 in axons and was not significantly different from negative controls in the dendritic compartment (Fig. 8B). Intriguingly, in comparison with wild-type KIF2A.1, the mutants KIF2A^{S317N} and KIF2A^{H321D} showed a drastic reduction in mitochondrial co-localization in soma, axons and dendrites (Fig. 8C,D). These results are generally consistent with our BioID findings, in which KIF2A.1 and KIF2A.2 isoforms displayed the largest number of mitochondrial proteins in their interactome datasets.

Mitochondrial localization to neuronal processes is unchanged in cortical neurons of *Kif2a* knockout mice (Homma et al., 2003). Considering the possibility of compensatory mechanisms that might operate during a relatively longer period of brain development in mice, we asked whether an acute depletion of KIF2A in primary cortical neurons would cause mitochondrial localization defects. After co-transfection with *shKif2a* and mCherry-TOMM20, we quantified mCherry signal in neuronal soma, axon and dendrites.

Development (2021) 148, dev192674. doi:10.1242/dev.192674

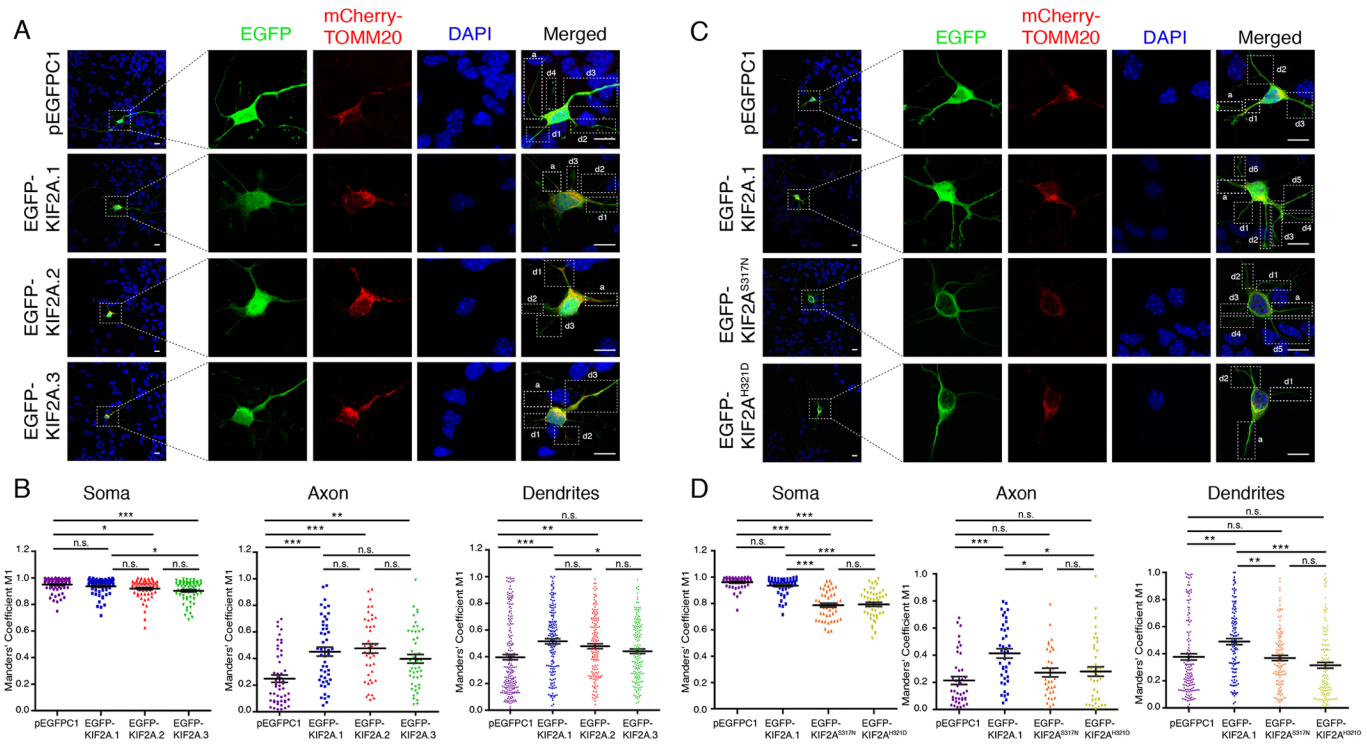

Fig. 8. KIF2A isoforms and *Kif2a* disease mutants display different levels of co-localization with mitochondria. (A,C) Primary cortical neurons from E14.5 embryos co-transfected at 2 DIV with mCherry-TOMM20-N-10 plasmid along with pEGFPC1 backbone vector or one of the EGFP-tagged KIF2A isoforms (A) or EGFP-tagged KIF2A mutants (C). Neurons were fixed at 4 DIV and immunostained against EGFP. Mitochondria were visualized using the mCherry reporter. Axon (a) and dendrites (d1-n) used for quantification are indicated with boxed areas in magnified and merged channel. (B,D) Quantification of co-localization of mCherry-labeled mitochondria with EGFP-tagged KIF2A isoforms (B) and KIF2A mutants (D) in soma, axon and dendrites using Manders' coefficient (M1) (Dunn et al., 2011; Manders et al., 1993; Zinchuk and Zinchuk, 2008): the fraction of mCherry (mitochondria) fluorescence overlapped with EGFP (KIF2A) fluorescence. *n*=65 for pEGFPC1, KIF2A.1 and KIF2A.3, *n*=63 for KIF2A.2 (in B); *n*=50 for pEGFPC1 and KIF2A.1, *n*=49 for KIF2A^{S317N} and KIF2A^{H321D} (in D). Data are mean±s.e.m. **P*<0.05, ***P*<0.005, ****P*<0.0001 (one-way ANOVA with post-hoc Tukey's multiple comparison test). n.s., non-significant. Scale bars: 10 µm.

Our results show that mitochondrial localization in these compartments is comparable between *Kif2a* silenced and control neurons (Fig. S9). Taken together, our results suggest a potential isoform-specific interaction between KIF2A and mitochondria, specifically in the axonal and dendritic compartments of neurons. The potential functional role of these interactions remain to be solved in the future.

DISCUSSION

Kif2a is an alternatively spliced gene, and isoform abundance is developmentally regulated (Ince-Dunn et al., 2012; Zhang et al., 2016). Here, we reveal that all three KIF2A isoforms can rescue a dendritic pruning defect caused by knockdown of all KIF2A expression in cortical neurons. However, only KIF2A.1 and KIF2A.2, but not KIF2A.3, are able to support migration of neurons in the developing cortex. KIF2A.3 differs from the other two isoforms by a 20 amino acid-long serine-rich disordered protein region located immediately N-terminal to its dimerization domain. Currently, we do not know how this short stretch of amino acids affects KIF2A function and how these functional changes might impact neural progenitor division or neuronal migration in the developing cortex. However, the results from our isoform-specific proximity-labeling screen demonstrated that the protein interactome of KIF2A.3 is significantly different from the other two isoforms.

Our BioID assay for KIF2A carried out in a neuronal cell line identified a number of centrosomal proteins with roles in bipolar spindle assembly, of which NUMA and CEP170 are known KIF2A interactors (Gaetz and Kapoor, 2004; Welburn and Cheeseman, 2012; Zhang et al., 2019). In mitotic cells KIF2A is essential for bipolar spindle assembly and at the poles it depolymerizes minus-end MTs to contribute to poleward chromosome movement (Ali et al., 2017; Ganem and Compton, 2004; Manning et al., 2007). Here, we provide additional candidate KIF2A-interacting proteins such as KMT2E, CKAP5, RANBP2 and CHD4, which also localize to bipolar spindles. Further investigations on how KIF2A and these candidate proteins functionally interact is likely to provide new mechanistic understanding of bipolar spindle assembly and chromosome segregation. These interactions may be particularly relevant for dividing neural progenitors in the VZ of the developing cortex.

We also identified unexpected KIF2A interactors such as a number of proteins targeted to organelles, mostly to the mitochondria, RNA processing enzymes and translation factors. We recognize that a subset of these hits may represent potential contaminants in our dataset. However, given that many of them display clear isoform-specificity we wish to speculate on the exciting implications of these findings. Several of these proteins have well-described roles in MT-based cargo trafficking. Interestingly, the original biochemical characterization of KIF2A revealed clear interactions with vesicle structures in neurons that were distinct from synaptic vesicles (Noda et al., 1995). It is possible that organelle and vesicle trafficking appear to be unaffected in *Kif2a* knockout cells (Homma et al., 2003) owing to genetic redundancy with other kinesins. In support of this idea, our BioID results identify KTN1 and TRAK1, which are both kinesin

Development (2021) 148, dev192674. doi:10.1242/dev.192674

adaptor proteins with essential roles in mitochondrial transport along MTs, as potential KIF2A interactors (Barel et al., 2017; Brickley and Stephenson, 2011; López-Doménech et al., 2018; MacAskill et al., 2009; Tanaka et al., 1998).

Perhaps the most interesting aspect of these unexpected hits is the fact that mitochondrial proteins are enriched in KIF2A.1 and KIF2A.2 interactomes and largely reduced in the dataset from KIF2A.3, the isoform which cannot support neuronal migration. Furthermore, we observed new candidates (such as SRP68, PES1 and EIF4ENIF1) that are only identified in the interactome of KIF2A.3. Consistent with our BioID analysis we further confirm that indeed KIF2A.1, KIF2A.2 and, to a much reduced extent, KIF2A.3 display mitochondrial co-localization in axons and dendrites of primary cortical neurons. Paradoxically, KIF2A does not harbor a mitochondrial-targeting sequence, is not listed as a mitochondrial protein in a mitochondrial proteome database (Calvo et al., 2016) and mitochondrial distribution is not affected in *Kif2a* knockout cells (Homma et al., 2003). Currently we do not know whether and how KIF2A-mitochondria co-localization affects mitochondrial trafficking, protein targeting or its metabolic functions. Intriguingly, several important studies have uncovered a role for MT- and kinesin-based trafficking of ribosome-associated mRNA complexes targeted to the mitochondrial surface for co-translational mitochondrial import (Fazal et al., 2019; Gagnon and Mowry, 2011; Kanai et al., 2004; Messitt et al., 2008). Whether KIF2A plays a direct role in MT-based RNA-protein complex transport, or might generally be in close proximity to a number of MT-associated-cargo due to its function in MT depolymerization, remains to be discovered.

Previous findings have demonstrated an essential role for KIF2A in axonal pruning (Homma et al., 2003; Maor-Nof et al., 2013), neuronal migration (Gilet et al., 2020; Homma et al., 2003) and in primary cilium disassembly during mitotic division of neural progenitors (Broix et al., 2018; Ding et al., 2019; Miyamoto et al., 2015; Zhang et al., 2019). As Neuro2A cells are actively dividing and do not possess primary cilia, our BioID assay did not identify primary cilium-specific proteins. However, several of the candidate KIF2A interactors are likely to have important functions during development of the cerebral cortex. For example, we have verified interactions between the neurite outgrowth inhibitor RTN4 and endogenous KIF2A in Neuro2A cells. Interestingly, RTN4 acts a negative regulator of radial neuron migration, and cortical lamination is defective in *Rtn4* knockout mice (Mathis et al., 2010). Among other interactors is CEP170, which is a KIF2A.2-specific interactor, regulates primary cilia disassembly and neural progenitor division in the VZ by functioning in a previously described WDR62-CEP170-KIF2A pathway (Zhang et al., 2019). CHD4 is a candidate interactor of KIF2A.1 and KIF2A.3 isoforms, and is a chromatin remodeling histone deacetylase, promoting the proliferation of neural progenitors at the cortical VZ during development (Nitarska et al., 2016). Finally, mutations in KMT2E, a lysine methyl transferase localized to spindle poles and a candidate interactor of all KIF2A isoforms, result in a range of neurodevelopmental disorders in humans, often manifesting with microcephaly and epilepsy (O'Donnell-Luria et al., 2019). Further characterization of these potential KIF2A interactors will reveal important details of how KIF2A controls early cortical development.

Mutations in the ATP binding sites of the KIF2A motor domain cause malformations of cortical development (Broix et al., 2018; Cavallin et al., 2017; Poirier et al., 2013; Tian et al., 2016). Patients manifest with a spectrum of symptoms which may include frontal band heterotopia, pachygyria, microcephaly, lissencephaly and neonatal onset seizure (Broix et al., 2018; Cavallin et al., 2017; Poirier et al., 2013; Tian et al., 2016). These mutations have been associated with severe migration defects of neurons in the developing cortex and defects in the MT depolymerization activity of KIF2A (Broix et al., 2018; Gilet et al., 2020), ability to regulate the structure and function of the MT-based structure the primary cilium and cell cycle defects in cortical neural progenitors (Broix et al., 2018). However, how these individual processes culminate in the symptomatic manifestations described in humans is unclear. Here, we investigated how one of these previously described motor domain patient mutations in KIF2A affect its interactome. Interestingly, we identified that the proximity-labeling-based interactome of KIF2A^{H321D} exhibits clear changes from its wild-type isoform (KIF2A.1). In particular, we observed a strong depletion of mitochondrial proteins in the interactome dataset of KIF2A^{H321D} and the presence of ectopic new proteins, the functions of which generally center on RNA regulation and transport. To date, few studies have investigated mitochondrial function in cortical neuron migration and lamination and have provided conflicting results. For example, although inhibition of mitochondrial protein adenine nucleotide transferase 1 (ANT1; SLC25A4) had no effects on cortical development (Lin-Hendel et al., 2016), knockout mice for mitochondria localized glutamic acid rich protein (*Mgarp*) showed defective radial migration and cortical axon and dendrite polarization, associated with abnormalities in motility and distribution of mitochondria (Jia et al., 2014). Our results suggest that a role for kinesins, and KIF2A in particular, in mitochondrial regulation during neuronal migration and cortical development should be investigated. Although further analysis is essential to resolve the biological relevance of our findings, the utility of our approach to identify potential interactors of different KIF2A isoforms and a mutant with relevance to pathogenesis of human cortical malformations is revealed.

MATERIALS AND METHODS

Cloning

Mouse *Kif2a.1*, *Kif2a.2* and *Kif2a.3* were cloned by reverse transcription from total RNA prepared from postnatal day (P) 0 mouse cortex, restriction digestion and ligation into the *EcoR*I/*Hind*III sites in the pEGFPC1 backbone vector. Subsequently myc-tagged versions of all isoforms and the mutants were subcloned into pcDNA4A-myc backbone vector using the *EcoR*I/*BamH*I sites. Mouse *Kif2a.1*, *Kif2a.2*, *Kif2a.3* and *Kif2a*^{H321D} were subcloned from the pEGFPC1 vector into *Xho*I/*EcoR*I sites of the pcDNA3.1(-)-mycBirA backbone vector (BirA*, N terminal; kindly provided by Elif N. Fırat-Karalar, Koç University, Istanbul). The primer sequences were as follows: Kif2a_BirAN_F (AAACTCGAGATGGTAAC-ATCTTTAAATGAAGAT); Kif2a_BirAN_R (AAAGAATTCTTAGAGG-GCTGGGGCCTCTTGGG). H321D and S317N point mutations were created by site-directed mutagenesis of mouse pEGFPC1-Kif2a.1. The primer sequences were as follows: Kif2a_c959G>A_F (GCAGACTGGA-AATGGGAAAACTCATACTATGG); Kif2a_c961C>G_F (GCAGACTG-GAAGTGGGAAAACTGATACTATGG); Kif2a_sdm_R (CCATAAGCA-AAGCACGTAGCCATGCCCCTTT). Non-silencing (NS) and *shKif2a* shRNA were cloned into pSUPER-neo-EGFP (www.oligoengine.com) as described in the manufacturer's manual. For *in utero* electroporation experiments, the EGFP cassette was exchanged with an mCherry cDNA by subcloning into the *Age*I/*Not*I sites of pSUPER-neo. Three isoforms of *shKif2a*-resistant cDNA (*resKif2a.1*, *resKif2a.2* and *resKif2a.3*) and mutants of *shKif2a*-resistant cDNA (*resKif2a*^{S317N} and *resKif2a*^{H321D}) were created by site-directed mutagenesis in a pcDNA4A backbone vector by introducing three silent mutations (A1521T, C1524G and T1527C) within the *shKif2a* target sequence (GGAATGGCATCCTGTGAAA) (Jang et al., 2008). The primer sequences were as follows: NS_F (GATCCCCGCGCGATAGCGC-TAATAATTTTTCAAGAGAAAATTATTAGCGCTATCGCGCTTTTTA); NS_R (AGTCTAAAAAGCGCGATAGCGCTAATAATTTTCTCTTGAA-AAATTATTAGCGCTATCGCGCGGG); shKif2a_F (GATCCCCGGAAT-

Development (2021) 148, dev192674. doi:10.1242/dev.192674

GGCATCCTGTGAAATTCAAGAGATTTCACAGGATGCCATTCCTTT-TTA); shKif2a_R (AGCTAAAAAGGAATGGCATCCTGTGAAATCTC-TTGAATTTCACAGGATGCCATTCCGGG); resKIF2A_F (CCAGGAA-TGGCTTCGTGCGAAAATACTCT); resKIF2A_R (AGAGATTGTGGC-AATCATGCAGGTACGAG). All constructs were confirmed by Sanger sequencing. mCherry-TOMM20-N-10 plasmid was acquired from Addgene (plasmid #55146).

Primary cortical cultures

Primary cortical cultures were prepared as previously described (Guner et al., 2017). Briefly, cortices from E14.5-E18.5 embryos were dissected in ice-cold 1× HBSS containing 10 mM HEPES and digested in 20 U/ml papain enzyme at 37°C for 10 min. We used 10 mg/ml trypsin inhibitor to terminate digestion. Tissue was washed with Basal Media Eagle supplemented with 0.5% L-glutamine, 1% penicillin/streptomycin and 5% fetal bovine serum (FBS) (BF) twice at room temperature and triturated three to five times. Then 300,000 cells were plated onto each well of a 24-well plate (pre-coated with laminin and poly-L-lysine) in BF. After 2 h incubation at 37°C, medium was changed into BF containing N-2 and B-27 supplements (Gibco Life Technologies).

Immunoassays

Neuro2A and HEK293T cells were maintained in EMEM and DMEM, respectively, and each was supplemented with 10% FBS, 1% penicillin/streptomycin and 0.5% L-glutamine (complete media). Plasmids were transfected into primary cortical neurons at 2 days *in vitro* (DIV) using Lipofectamine 2000 (Invitrogen), or HEK293T cells using Lipofectamine 3000 (Invitrogen), according to the manufacturer's protocol. Neuro2A cells were transfected using 1 mg/ml Polyethylenimine (PEI) dissolved in sterile water (Polysciences). For immunoblotting, protein lysates were collected 2 days after transfection either in ice-cold RIPA buffer [0.05 M Tris-HCl (pH 7.5), 0.15 M NaCl, 1% Triton X-100, 1% Na-DOC, 0.1% SDS] supplemented with protease inhibitor or Lysis Buffer [10 mM Tris-HCl (pH 7.6) containing 0.5% SDS, 2% NP-40, 150 mM NaCl, 1 mM EDTA] supplemented with 10 mM iodoacetamide and protease inhibitor. Antibodies and dilutions used were as follows: myc (Santa Cruz Biotechnology, SC-40, 1:1000); hnRNP C1+C2 (Abcam, ab10294, 1:2000); biotin (gift from Dr Timothy J. Mitchison, Harvard Medical School, Boston, MA, USA, 1:20,000); Histone H3 (Cell Signaling Technology, 9715S, 1:2500); β-actin (Abcam, ab6276, 1:5000); EGFP (Santa Cruz Biotechnology, sc-8334, 1:1000).

For immunofluorescence staining, both Neuro2A cells and primary cortical neurons were transfected with Lipofectamine 2000 (Invitrogen) 2 days after plating and fixed with 4% paraformaldehyde (PFA) 2 days after transfection. Neuro2A cells were imaged using a Leica DMI8 SP8 CS/DLS confocal microscope and LasX Life Science software. Primary cortical neurons were imaged using a Nikon Eclipse 90i confocal microscope and NIS-Elements AR software, and a Leica DMI8 SP8 CS/DLS confocal microscope and LasX Life Science software. For co-localization analysis, quantification was performed using JACoP plugin which calculates the Manders' Coefficients M1 and M2 and these values provide a direct measure of the quantity of interest independent of signal proportionality (Dunn et al., 2011; Manders et al., 1993; Zinchuk and Zinchuk, 2008). Sholl analysis was performed with the Sholl analysis plug-in in ImageJ software (Ferreira et al., 2014; Schindelin et al., 2012). Sholl analysis parameters are: 1 µm starting radius, 300 µm ending radius, 2 µm radius step size, 1 µm radius span, and span type, median. Antibodies and dilutions used were as follows: myc (Santa Cruz Biotechnology, SC-40, 1:1000); EGFP (Santa Cruz Biotechnology, sc-8334, 1:1000); GFP (Aves Labs, GFP-1020, 1:10,000); α-tubulin (Cell Signaling Technology, 3873S, 1:1000); β-III-tubulin (Tuj1) (Abcam, ab7751, 1:500); KIF2A (Abcam, ab71160, 1:1000); Streptavidin Alexa Fluor®488 conjugate (Life Technologies, S32354, 1:5000); RTN4 (Nogo C-4, Santa Cruz Biotechnology, sc-271878, 1:500); NEUROD2 (Abcam, ab168932, 1:1000); GFAP (Sigma-Aldrich, G3893, 1:200).

qRT-PCR

Mice cortices at different developmental time points (E14, E16, E18, P0, P7, P14, P21, P28 and adult) were collected in 1× cold HBSS and total RNA was isolated in Trizol (Thermo Fisher Scientific). cDNA was synthesized using Transcriptor High-Fidelity cDNA Synthesis Kit (Roche) and qRT-PCR was performed with Luminaris HiGreen qPCR Master Mix (Thermo Fisher Scientific) using a CFX Connect Real-Time PCR detection System (Bio-Rad). *Kif2a* mRNA levels were normalized to *Gapdh* mRNA using the $2^{-\Delta\Delta CT}$ method. The primer sequences were as follows: Gapdh_F (CGAC-TTCAACAGCAACTCCCATCTTCC); Gapdh_R (TGGGTGGTCCAGG-GTTTCTTACTCCTT); Kif2a.1_F (CCAGGGTGAAAGAATTGACTG); Kif2a.1_R (GCTTCATGGAAAGTGAACAGC); Kif2a.2_F (GCAAATA-GGGTGAAAGAATTGACTG); Kif2a.2_R (TCTGGGAGACAGCTTCA-TGG); Kif2a.1_ex5long_F (CTCCTTCACGTAGAAAATCCAATT); Kif2a.1_ex5long_R (GTCTCTGATCATACACATAATTTCGT); Kif2a.3_ex5short_F (CAGAATGCACGTAGAAAATCCAA); Kif2a.3_ex5short_R (TCTGAAGTCTCTGATCATACACATA).

In utero electroporation and image analysis

The *in utero* electroporation experiment was performed as previously described (Guzelsoy et al., 2019; Saito, 2006) using E14.5 pregnant CD1 mice. Briefly, timed pregnant mice (E14.5) were anesthetized using isoflurane. The uterine horns were exposed by laparotomy and lateral ventricle of each embryo was injected using pulled glass capillaries (Drummond® PCR micropipettes, pulled as 60 µm diameter) with 333 ng/µl NS (control) or *shKif2a* plasmids combined with 333 ng/µl *resKif2a.1*, *resKif2a.2* or *resKif2a.3* and 333 ng/µl pCAGGS_IRES_tdTomato to visualize transfected neurons and 0.1% Fast Green to monitor the injection (all plasmids were prepared using Qiagen Endofree Plasmid Maxi Kit). Plasmid DNA was electroporated into the neuronal progenitors located in the VZ by 0.5 pulses at 30 V for 400 ms intervals with an electroporator (BTX Harvard Apparatus, ECM830) using 5 mm tweezertrodes (BTX Harvard Apparatus). Uterine horns were placed back in the abdominal cavity, and development of embryos was allowed to continue for 3 days (E17.5). Embryo brains were harvested and fixed with 4% PFA in PBS overnight at 4°C. Brains were sectioned coronally at 50 µm using a cryostat (CM1950, Leica Biosystems). Optical *z*-series through 50 µm images were captured using a Leica DMI8 SP8 CS/DLS microscope and maximum intensity projections were generated in LasX Life Science software. Images were opened in Photoshop CC (Adobe Systems) for positioning the ten bins grid for the cell counting. Number of transfected cells were counted for each bin using the cell counter option of ImageJ (National Institutes of Health; Schindelin et al., 2012) and then data were transferred to Excel (Microsoft) for further analysis. Bins 1-5 represent CP, bins 6-9 represent SVZ-IZ and bin 10 represents VZ. Finally, graphs were plotted using GraphPad Prism 5 software.

Proximity-dependent biotinylation and mass spectrometry analysis (BioID)

Neuro2A cells were transfected with 60 µg BioID constructs using 1 mg/ml PEI. The following day, medium was changed with complete EMEM containing 0.05 mM D-biotin (Life Technologies) and 1 mM ATP. Then, 2 days after transfection, protein lysates were collected in Lysis Buffer supplemented with 10 mM iodoacetamide and protease inhibitor by lysing the cells using an insulin syringe seven times. Protein concentration was measured by BCA Assay (Thermo Fisher Scientific) and equal amounts of protein from each condition was mixed with an equal volume of Streptavidin Plus UltraLink® Resin (Pierce®), which was pre-washed with 1× PBS and Lysis Buffer. Proteins were incubated with streptavidin beads overnight at 4°C on a tube rotator. In order to eliminate sample loss, on-bead digestion for streptavidin-captured biotinylated proteins was performed the following day. Beads were washed with Wash buffers 1, 2, 3 and 4 twice for 10 min each [Wash Buffer 1: 2% SDS; Wash Buffer 2: 2% Na-DOC, 1% Triton X-100, 50 mM NaCl, 50 mM HEPES (pH 7.5), 1 mM EDTA; Wash Buffer 3: 0.5% NP-40, 0.5% Na-DOC, 1% Triton X-100, 500 mM NaCl, 1 mM EDTA, 10 mM Tris-HCl (pH 8.1); Wash Buffer 4: 50 mM Tris-HCl (pH 7.4), 50 mM NaCl]. For the affinity capture experiment followed by immunoblotting, proteins were eluted with elution buffer (500 nM D-biotin in 2× Laemmli Buffer with 0.1 M DTT) at 98°C for 10 min with 1000 rpm shaking.

For the identification of biotinylated proteins by mass spectrometry, beads were washed with urea solution [8 M urea in 0.1 M Tris-HCl (pH 8.5)] and then reduced with DTT (100 mM in urea solution) at 56°C for 30 min. Beads

were washed with urea solution and then incubated with iodoacetamide (0.05 M in urea solution) for 20 min in the dark for alkylation of cysteine residues. Beads were washed with urea solution and 0.05 M ammonium bicarbonate solution (NH_4HCO_3) (0.05 M in HPLC grade water) twice for each buffer. For 600 µg of protein digestion, 4 µg of trypsin (MS Grade Trypsin Protease, Pierce) was added to beads for 16 h at 37°C with 1000 rpm shaking. Peptides were treated with 10% acetic acid in order to terminate trypsin digestion and peptides were eluted using C18 stage tips (Rappsilber et al., 2007). Eluates were dried in a speed vacuum system (Thermo Fisher Scientific Radiant Cover, rc110b) and were analyzed using a Q-Exactive LC-MS/MS mass spectrometer (Thermo Fisher Scientific). The datasets were analyzed against the *Mus musculus* Swissprot/Uniprot database (UniProt, 2019). For analysis, the spectral counts of proteins were used to calculate fold change ratios and FDR values for each KIF2A isoform and KIF2A^{H321D} mutant using the qspec-param program of qprot_v1.3.5. Proteins found in less than two biological replicates were filtered away. Proteins with the same gene name were merged via sum of PSM values. Normalization methods, *z*-statistics and FDR values were calculated as previously described (Choi et al., 2015). Proteins were filtered out if FDR>0.05 or fold change<1.5. Heat map was created with Prism 8. For cluster analysis, significant protein hits were analyzed using the String database v11.0 (Szklarczyk et al., 2019) by Cytoscape StringApp (Doncheva et al., 2019) with 0.4 confidence. Affinity propagation clustering of the network was performed by Cytoscape (version 3.7.2) and its plugin clustermaker (Cline et al., 2007). GO and KEGG enrichment analysis of the network was performed via g:Profiler (Raudvere et al., 2019).

PLA

Neuro2A cells were plated on 24-well plates with coverslips. The PLA was performed using Duolink® In Situ Red Starter Kit Mouse/Rabbit (DUO92101, Sigma-Aldrich) according to the manufacturer's protocol. Briefly, cells were fixed with 3.2% PFA for 15 min and blocked with Duolink® Blocking Solution for 30 min at 37°C. Cells were incubated with primary antibody pairs or only one primary antibody in Duolink® antibody diluent overnight at 4°C. Cells were washed with Wash Buffer A and incubated with Duolink® Plus and Minus PLA probes in antibody diluent for 1 h at 37°C. Cells were washed with Wash Buffer A and ligation was performed using ligase diluted in Duolink® Ligation buffer for 30 min at 37°C followed by washes with Wash buffer A. Amplification was performed with polymerase diluted in Duolink® Amplification buffer for 100 min at 37°C. Cells were washed with Wash buffer B followed by 0.01× Wash buffer B and finally mounted with mounting medium containing DAPI. Images were captured with a Leica DMI8 SP8 CS/DLS microscope using the DAPI channel to observe nuclei and the red channel (λex 594 nm; λem 624 nm) to observe PLA dots. Optical *z*-series images were projected into a flattened plane with the maximum intensity option of the LasX Life Science software. Image analysis was performed with ImageJ software (Debaize et al., 2017). Antibodies and dilutions used were as follows: KIF2A (Abcam, ab71160 1:5000); RTN4 (Nogo C-4, Santa Cruz Biotechnology, sc-271878, 1:500).

Use of animals

All animal experiments were performed in accordance with the guidelines for the care and use of laboratory animals of Koç University and the Ministries of Food, Agriculture and Livestock, Forestry and Water Management of Turkey. All mice were bred, maintained and housed at the Koç University Animal Facility. Ethics approval was obtained from Koç University Institutional Animal Care and Use Committee (license no. 2014–9).

Acknowledgements

We thank Ahmet Kocabay, Nilhan Coskun, Mustafa Demir and Muhammed Resat Oguzkan Yaralı (Koç University Animal Research Facility, Turkey) for their help in providing timed pregnant mice; the Molecular Imaging Core Facility of Koç University Research Center for Translational Medicine (KUTTAM), Berna Morova, Alper Kiraz from Koç University College of Science and Dr Sercin Karahuseyinoglu from KUTTAM for assistance with confocal microscopy; and Cory Dunn for feedback on the manuscript.

Competing interests

The authors declare no competing or financial interests.

Author contributions

Conceptualization: C.A., G.I.-D.; Formal analysis: A.K., C.A., G.I.-D.; Investigation: C.A., D.A., B.A.A., G.G., E.B., N.O., G.I.-D.; Writing - original draft: C.A., G.I.-D.; Project administration: A.C.T., N.O., G.I.-D.

Funding

This work was funded by a European Commission Seventh Framework Programme International Reintegration Grant (PIRG07-GA-2010-268433 to G.I.-D.) and Türkiye Bilimsel ve Teknolojik Araştırma Kurumu (TUBITAK-115Z707 to G.I.-D.; TUBITAK-BIDEB 2211/E Scholarship Program to C.A.).

Supplementary information

Supplementary information available online at
https://dev.biologists.org/lookup/doi/10.1242/dev.192674.supplemental

Peer review history

The peer review history is available online at
https://dev.biologists.org/lookup/doi/10.1242/dev.192674.reviewer-comments.pdf

References

Ali, A., Veeranki, S. N., Chinchole, A. and Tyagi, S. (2017). MLL/WDR5 complex regulates Kif2A localization to ensure chromosome congression and proper spindle assembly during mitosis. *Dev. Cell* **41**, 605-622.e7. doi:10.1016/j.devcel.2017.05.023

Barel, O., Malicdan, M. C. V., Ben-Zeev, B., Kandel, J., Pri-Chen, H., Stephen, J., Castro, I. G., Metz, J., Atawa, O., Moshkovitz, S. et al. (2017). Deleterious variants in TRAK1 disrupt mitochondrial movement and cause fatal encephalopathy. *Brain : A J. Neurol.* **140**, 568-581. doi:10.1093/brain/awx002

Brickley, K. and Stephenson, F. A. (2011). Trafficking kinesin protein (TRAK)-mediated transport of mitochondria in axons of hippocampal neurons. *J. Biol. Chem.* **286**, 18079-18092. doi:10.1074/jbc.M111.236018

Broix, L., Asselin, L., Silva, C. G., Ivanova, E. L., Tilly, P., Gilet, J. G., Lebrun, N., Jagline, H., Muraca, G., Saillour, Y. et al. (2018). Ciliogenesis and cell cycle alterations contribute to KIF2A-related malformations of cortical development. *Hum. Mol. Genet.* **27**, 224-238. doi:10.1093/hmg/ddx384

Buljan, M., Chalancon, G., Dunker, A. K., Bateman, A., Balaji, S., Fuxreiter, M. and Babu, M. M. (2013). Alternative splicing of intrinsically disordered regions and rewiring of protein interactions. *Curr. Opin. Struct. Biol.* **23**, 443-450. doi:10.1016/j.sbi.2013.03.006

Calvo, S. E., Clauser, K. R. and Mootha, V. K. (2016). MitoCarta2.0: an updated inventory of mammalian mitochondrial proteins. *Nucleic Acids Res.* **44**, D1251-D1257. doi:10.1093/nar/gkv1003

Cavallin, M., Bijlsma, E. K., El Morjani, A., Moutton, S., Peeters, E. A. J., Maillard, C., Pedespan, J. M., Guerrot, A.-M., Drouin-Garaud, V., Coubes, C. et al. (2017). Recurrent KIF2A mutations are responsible for classic lissencephaly. *Neurogenetics* **18**, 73-79. doi:10.1007/s10048-016-0499-8

Choi, H., Kim, S., Fermin, D., Tsou, C.-C. and Nesvizhskii, A. I. (2015). QPROT: statistical method for testing differential expression using protein-level intensity data in label-free quantitative proteomics. *J. Proteomics* **129**, 121-126. doi:10.1016/j.jprot.2015.07.036

Cline, M. S., Smoot, M., Cerami, E., Kuchinsky, A., Landys, N., Workman, C., Christmas, R., Avila-Campilo, I., Creech, M., Gross, B. et al. (2007). Integration of biological networks and gene expression data using Cytoscape. *Nat. Protoc.* **2**, 2366-2382. doi:10.1038/nprot.2007.324

Debaize, L., Jakobczyk, H., Rio, A.-G., Gandemer, V. and Troadec, M.-B. (2017). Optimization of proximity ligation assay (PLA) for detection of protein interactions and fusion proteins in non-adherent cells: application to pre-B lymphocytes. *Mol. Cytogenet.* **10**, 27. doi:10.1186/s13039-017-0328-2

Dhananjaya, D., Hung, K.-Y. and Tarn, W.-Y. (2018). RBM4 modulates radial migration via alternative splicing of dab1 during cortex development. *Mol. Cell. Biol.* **38**, e00007-e00018. doi:10.1128/MCB.00007-18

Ding, W., Wu, Q., Sun, L., Pan, N. C. and Wang, X. (2019). Cenpj regulates cilia disassembly and neurogenesis in the developing mouse cortex. *J. Neurosci.* **39**, 1994-2010. doi:10.1523/JNEUROSCI.1849-18.2018

Doncheva, N. T., Morris, J. H., Gorodkin, J. and Jensen, L. J. (2019). Cytoscape StringApp: network analysis and visualization of proteomics data. *J. Proteome Res.* **18**, 623-632. doi:10.1021/acs.jproteome.8b00702

Dosztányi, Z. (2018). Prediction of protein disorder based on IUPred. *Protein Sci.* **27**, 331-340. doi:10.1002/pro.3334

Dunn, K. W., Kamocka, M. M. and McDonald, J. H. (2011). A practical guide to evaluating colocalization in biological microscopy. *Am. J. Physiol.-Cell Physiol.* **300**, C723-C742. doi:10.1152/ajpcell.00462.2010

Ellis, J. D., Barrios-Rodiles, M., Çolak, R., Irimia, M., Kim, T., Calarco, J. A., Wang, X., Pan, Q., O'Hanlon, D., Kim, P. M. et al. (2012). Tissue-specific alternative splicing remodels protein-protein interaction networks. *Mol. Cell* **46**, 884-892. doi:10.1016/j.molcel.2012.05.037

Fazal, F. M., Han, S., Parker, K. R., Kaewsapsak, P., Xu, J., Boettiger, A. N., Chang, H. Y. and Ting, A. Y. (2019). Atlas of subcellular RNA localization revealed by APEX-seq. *Cell* **178**, 473-490.e26. doi:10.1016/j.cell.2019.05.027

Ferreira, T. A., Blackman, A. V., Oyrer, J., Jayabal, S., Chung, A. J., Watt, A. J., Sjöström, P. J. and van Meyel, D. J. (2014). Neuronal morphometry directly from bitmap images. *Nat. Methods* **11**, 982-984. doi:10.1038/nmeth.3125

Gaetz, J. and Kapoor, T. M. (2004). Dynein/dynactin regulate metaphase spindle length by targeting depolymerizing activities to spindle poles. *J. Cell Biol.* **166**, 465-471. doi:10.1083/jcb.200404015

Gagnon, J. A. and Mowry, K. L. (2011). Molecular motors: directing traffic during RNA localization. *Crit. Rev. Biochem. Mol. Biol.* **46**, 229-239. doi:10.3109/10409238.2011.572861

Ganem, N. J. and Compton, D. A. (2004). The KinI kinesin Kif2a is required for bipolar spindle assembly through a functional relationship with MCAK. *J. Cell Biol.* **166**, 473-478. doi:10.1083/jcb.200404012

Gilet, J. G., Ivanova, E. L., Trofimova, D., Rudolf, G., Meziane, H., Broix, L., Drouot, N., Courraud, J., Skory, V., Voulleminot, P. et al. (2020). Conditional switching of KIF2A mutation provides new insights into cortical malformation pathogeny. *Hum. Mol. Genet.* **29**, 766-784. doi:10.1093/hmg/ddz316

Guner, G., Guzelsoy, G., Isleyen, F. S., Sahin, G. S., Akkaya, C., Bayam, E., Kotan, E. I., Kabakcioglu, A. and Ince-Dunn, G. (2017). NEUROD2 regulates stim1 expression and store-operated calcium entry in cortical neurons. *eNeuro* **4**, ENEURO.0255-16.2017. doi:10.1523/ENEURO.0255-16.2017

Guzelsoy, G., Akkaya, C., Atak, D., Dunn, C. D., Kabakcioglu, A., Ozlu, N. and Ince-Dunn, G. (2019). Terminal neuron localization to the upper cortical plate is controlled by the transcription factor NEUROD2. *Sci. Rep.* **9**, 19697. doi:10.1038/s41598-019-56171-x

Homma, N., Takei, Y., Tanaka, Y., Nakata, T., Terada, S., Kikkawa, M., Noda, Y. and Hirokawa, N. (2003). Kinesin superfamily protein 2A (KIF2A) functions in suppression of collateral branch extension. *Cell* **114**, 229-239. doi:10.1016/S0092-8674(03)00522-1

Homma, N., Zhou, R., Naseer, M. I., Chaudhary, A. G., Al-Qahtani, M. H. and Hirokawa, N. (2018). KIF2A regulates the development of dentate granule cells and postnatal hippocampal wiring. *eLife* **7**, e30935. doi:10.7554/eLife.30935

Ince-Dunn, G., Okano, H. J., Jensen, K. B., Park, W.-Y., Zhong, R., Ule, J., Mele, A., Fak, J. J., Yang, C., Zhang, C. et al. (2012). Neuronal Elav-like (Hu) proteins regulate RNA splicing and abundance to control glutamate levels and neuronal excitability. *Neuron* **75**, 1067-1080. doi:10.1016/j.neuron.2012.07.009

Irimia, M., Weatheritt, R. J., Ellis, J. D., Parikshak, N. N., Gonatopoulos-Pournatzis, T., Babor, M., Quesnel-Vallières, M., Tapial, J., Raj, B., O'Hanlon, D. et al. (2014). A highly conserved program of neuronal microexons is misregulated in autistic brains. *Cell* **159**, 1511-1523. doi:10.1016/j.cell.2014.11.035

Jang, C.-Y., Wong, J., Coppinger, J. A., Seki, A., Yates, J. R., Illrd and Fang, G. (2008). DDA3 recruits microtubule depolymerase Kif2a to spindle poles and controls spindle dynamics and mitotic chromosome movement. *J. Cell Biol.* **181**, 255-267. doi:10.1083/jcb.200711032

Jia, L., Liang, T., Yu, X., Ma, C. and Zhang, S. (2014). MGARP regulates mouse neocortical development via mitochondrial positioning. *Mol. Neurobiol.* **49**, 1293-1308. doi:10.1007/s12035-013-8602-8

Kanai, Y., Dohmae, N. and Hirokawa, N. (2004). Kinesin transports RNA: isolation and characterization of an RNA-transporting granule. *Neuron* **43**, 513-525. doi:10.1016/j.neuron.2004.07.022

Kandoi, G. and Dickerson, J. A. (2019). Tissue-specific mouse mRNA isoform networks. *Sci. Rep.* **9**, 13949. doi:10.1038/s41598-019-50119-x

Kriegstein, A. R. and Noctor, S. C. (2004). Patterns of neuronal migration in the embryonic cortex. *Trends Neurosci.* **27**, 392-399. doi:10.1016/j.tins.2004.05.001

Lin-Hendel, E. G., McManus, M. J., Wallace, D. C., Anderson, S. A. and Golden, J. A. (2016). Differential mitochondrial requirements for radially and non-radially migrating cortical neurons: implications for mitochondrial disorders. *Cell Rep.* **15**, 229-237. doi:10.1016/j.celrep.2016.03.024

López-Doménech, G., Covill-Cooke, C., Ivankovic, D., Halff, E. F., Sheehan, D. F., Norkett, R., Birsa, N. and Kittler, J. T. (2018). Miro proteins coordinate microtubule- and actin-dependent mitochondrial transport and distribution. *EMBO J.* **37**, 321-336. doi:10.15252/embj.201696380

MacAskill, A. F., Rinholm, J. E., Twelvetrees, A. E., Arancibia-Carcamo, I. L., Muir, J., Fransson, A., Aspenstrom, P., Attwell, D. and Kittler, J. T. (2009). Miro1 is a calcium sensor for glutamate receptor-dependent localization of mitochondria at synapses. *Neuron* **61**, 541-555. doi:10.1016/j.neuron.2009.01.030

Manders, E. M. M., Verbeek, F. J. and Aten, J. A. (1993). Measurement of co-localization of objects in dual-colour confocal images. *J. Microsc.* **169**, 375-382. doi:10.1111/j.1365-2818.1993.tb03313.x

Manning, A. L., Ganem, N. J., Bakhoum, S. F., Wagenbach, M., Wordeman, L. and Compton, D. A. (2007). The Kinesin-13 proteins Kif2a, Kif2b, and Kif2c/MCAK have distinct roles during mitosis in human cells. *Mol. Biol. Cell* **18**, 2970-2979. doi:10.1091/mbc.e07-02-0110

Maor-Nof, M., Homma, N., Raanan, C., Nof, A., Hirokawa, N. and Yaron, A. (2013). Axonal pruning is actively regulated by the microtubule-destabilizing protein kinesin superfamily protein 2A. *Cell Reports* **3**, 971-977. doi:10.1016/j.celrep.2013.03.005

Mathis, C., Schröter, A., Thallmair, M. and Schwab, M. E. (2010). Nogo-a regulates neural precursor migration in the embryonic mouse cortex. *Cereb. Cortex* **20**, 2380-2390. doi:10.1093/cercor/bhp307

Messitt, T. J., Gagnon, J. A., Kreiling, J. A., Pratt, C. A., Yoon, Y. J. and Mowry, K. L. (2008). Multiple kinesin motors coordinate cytoplasmic RNA transport on a subpopulation of microtubules in Xenopus oocytes. *Dev. Cell* **15**, 426-436. doi:10.1016/j.devcel.2008.06.014

Miyamoto, T., Hosoba, K., Ochiai, H., Royba, E., Izumi, H., Sakuma, T., Yamamoto, T., Dynlacht, B. D. and Matsuura, S. (2015). The microtubule-depolymerizing activity of a mitotic kinesin protein KIF2A drives primary cilia disassembly coupled with cell proliferation. *Cell Rep.* **10**, 664-673. doi:10.1016/j.celrep.2015.01.003

Nitarska, J., Smith, J. G., Sherlock, W. T., Hillege, M. M. G., Nott, A., Barshop, W. D., Vashisht, A. A., Wohlschlegel, J. A., Mitter, R. and Riccio, A. (2016). A functional switch of NuRD chromatin remodeling complex subunits regulates mouse cortical development. *Cell Rep.* **17**, 1683-1698. doi:10.1016/j.celrep.2016.10.022

Noda, Y., Sato-Yoshitake, R., Kondo, S., Nangaku, M. and Hirokawa, N. (1995). KIF2 is a new microtubule-based anterograde motor that transports membranous organelles distinct from those carried by kinesin heavy chain or KIF3A/B. *J. Cell Biol.* **129**, 157-167. doi:10.1083/jcb.129.1.157

O'Donnell-Luria, A. H., Pais, L. S., Faundes, V., Wood, J. C., Sveden, A., Luria, V., Abou Jamra, R., Accogli, A., Amburgey, K., Anderlid, B. M. et al. (2019). Heterozygous variants in KMT2E cause a spectrum of neurodevelopmental disorders and epilepsy. *Am. J. Hum. Genet.* **104**, 1210-1222. doi:10.1016/j.ajhg.2019.03.021

Pan, Q., Shai, O., Lee, L. J., Frey, B. J. and Blencowe, B. J. (2008). Deep surveying of alternative splicing complexity in the human transcriptome by high-throughput sequencing. *Nat. Genet.* **40**, 1413-1415. doi:10.1038/ng.259

Poirier, K., Lebrun, N., Broix, L., Tian, G., Saillour, Y., Boscheron, C., Parrini, E., Valence, S., Pierre, B. S., Oger, M. et al. (2013). Mutations in TUBG1, DYNC1H1, KIF5C and KIF2A cause malformations of cortical development and microcephaly. *Nat. Genet.* **45**, 639-647. doi:10.1038/ng.2613

Raj, B. and Blencowe, B. J. (2015). Alternative splicing in the mammalian nervous system: recent insights into mechanisms and functional roles. *Neuron* **87**, 14-27. doi:10.1016/j.neuron.2015.05.004

Rappsilber, J., Mann, M. and Ishihama, Y. (2007). Protocol for micro-purification, enrichment, pre-fractionation and storage of peptides for proteomics using stagetips. *Nat. Protoc.* **2**, 1896-1906. doi:10.1038/nprot.2007.261

Raudvere, U., Kolberg, L., Kuzmin, I., Arak, T., Adler, P., Peterson, H. and Vilo, J. (2019). g:Profiler: a web server for functional enrichment analysis and conversions of gene lists (2019 update). *Nucleic Acids Res.* **47**, W191-W198. doi:10.1093/nar/gkz369

Roux, K. J., Kim, D. I. and Burke, B. (2013). BioID: a screen for protein-protein interactions. **74**, 19.23.11-19.23.14. doi:10.1002/0471140864.ps1923s74

Saito, T. (2006). In vivo electroporation in the embryonic mouse central nervous system. *Nat. Protoc.* **1**, 1552-1558. doi:10.1038/nprot.2006.276

Schindelin, J., Arganda-Carreras, I., Frise, E., Kaynig, V., Longair, M., Pietzsch, T., Preibisch, S., Rueden, C., Saalfeld, S., Schmid, B. et al. (2012). Fiji: an open-source platform for biological-image analysis. *Nat. Methods* **9**, 676-682. doi:10.1038/nmeth.2019

Scotti, M. M. and Swanson, M. S. (2016). RNA mis-splicing in disease. *Nat. Rev. Genet.* **17**, 19-32. doi:10.1038/nrg.2015.3

Su, C.-H., Dhananjaya, D. and Tarn, W.-Y. (2018). Alternative splicing in neurogenesis and brain development. *Front. Mol. Biosci.* **5**, 12. doi:10.3389/fmolb.2018.00012

Szklarczyk, D., Gable, A. L., Lyon, D., Junge, A., Wyder, S., Huerta-Cepas, J., Simonovic, M., Doncheva, N. T., Morris, J. H., Bork, P. et al. (2019). STRING v11: protein–protein association networks with increased coverage, supporting functional discovery in genome-wide experimental datasets. *Nucleic Acids Res.* **47**, D607-D613. doi:10.1093/nar/gky1131

Tanaka, Y., Kanai, Y., Okada, Y., Nonaka, S., Takeda, S., Harada, A. and Hirokawa, N. (1998). Targeted disruption of mouse conventional kinesin heavy chain kif5b, results in abnormal perinuclear clustering of mitochondria. *Cell* **93**, 1147-1158. doi:10.1016/S0092-8674(00)81459-2

Tian, G., Cristancho, A. G., Dubbs, H. A., Liu, G. T., Cowan, N. J. and Goldberg, E. M. (2016). A patient with lissencephaly, developmental delay, and infantile spasms, due to de novo heterozygous mutation of KIF2A. *Mol. Genet. Genomic Med.* **4**, 599-603. doi:10.1002/mgg3.236

UniProt, C. (2019). UniProt: a worldwide hub of protein knowledge. *Nucleic Acids Res.* **47**, D506-D515. doi:10.1093/nar/gky1049

Urbanska, M., Blazejczyk, M. and Jaworski, J. (2008). Molecular basis of dendritic arborization. *Acta Neurobiol. Exp.* **68**, 264-288.

Wang, E. T., Sandberg, R., Luo, S., Khrebtukova, I., Zhang, L., Mayr, C., Kingsmore, S. F., Schroth, G. P. and Burge, C. B. (2008). Alternative isoform regulation in human tissue transcriptomes. *Nature* **456**, 470-476. doi:10.1038/nature07509

Welburn, J. P. I. and Cheeseman, I. M. (2012). The microtubule-binding protein Cep170 promotes the targeting of the kinesin-13 depolymerase Kif2b to the mitotic spindle. *Mol. Biol. Cell* **23**, 4786-4795. doi:10.1091/mbc.e12-03-0214

Yeo, G., Holste, D., Kreiman, G. and Burge, C. B. (2004). Variation in alternative splicing across human tissues. *Genome Biol.* **5**, R74. doi:10.1186/gb-2004-5-10-r74

Zhang, Y., Chen, K., Sloan, S. A., Bennett, M. L., Scholze, A. R., O'Keeffe, S., Phatnani, H. P., Guarnieri, P., Caneda, C., Ruderisch, N. et al. (2014). An RNA-sequencing transcriptome and splicing database of glia, neurons, and vascular cells of the cerebral cortex. *J. Neurosci.* **34**, 11929-11947. doi:10.1523/JNEUROSCI.1860-14.2014

Zhang, X., Chen, M. H., Wu, X., Kodani, A., Fan, J., Doan, R., Ozawa, M., Ma, J., Yoshida, N., Reiter, J. F. et al. (2016). Cell-type-specific alternative splicing governs cell fate in the developing cerebral cortex. *Cell* **166**, 1147-1162.e15. doi:10.1016/j.cell.2016.07.025

Zhang, W., Yang, S.-L., Yang, M., Herrlinger, S., Shao, Q., Collar, J. L., Fierro, E., Shi, Y., Liu, A., Lu, H. et al. (2019). Modeling microcephaly with cerebral organoids reveals a WDR62–CEP170–KIF2A pathway promoting cilium disassembly in neural progenitors. *Nat. Commun.* **10**, 2612. doi:10.1038/s41467-019-10497-2

Zinchuk, V. and Zinchuk, O. (2008). Quantitative colocalization analysis of confocal fluorescence microscopy images. *Curr. Protoc. Cell Biol.* **39**, 4.19.1-4.19.16. doi:10.1002/0471143030.cb0419s39

Figure S1

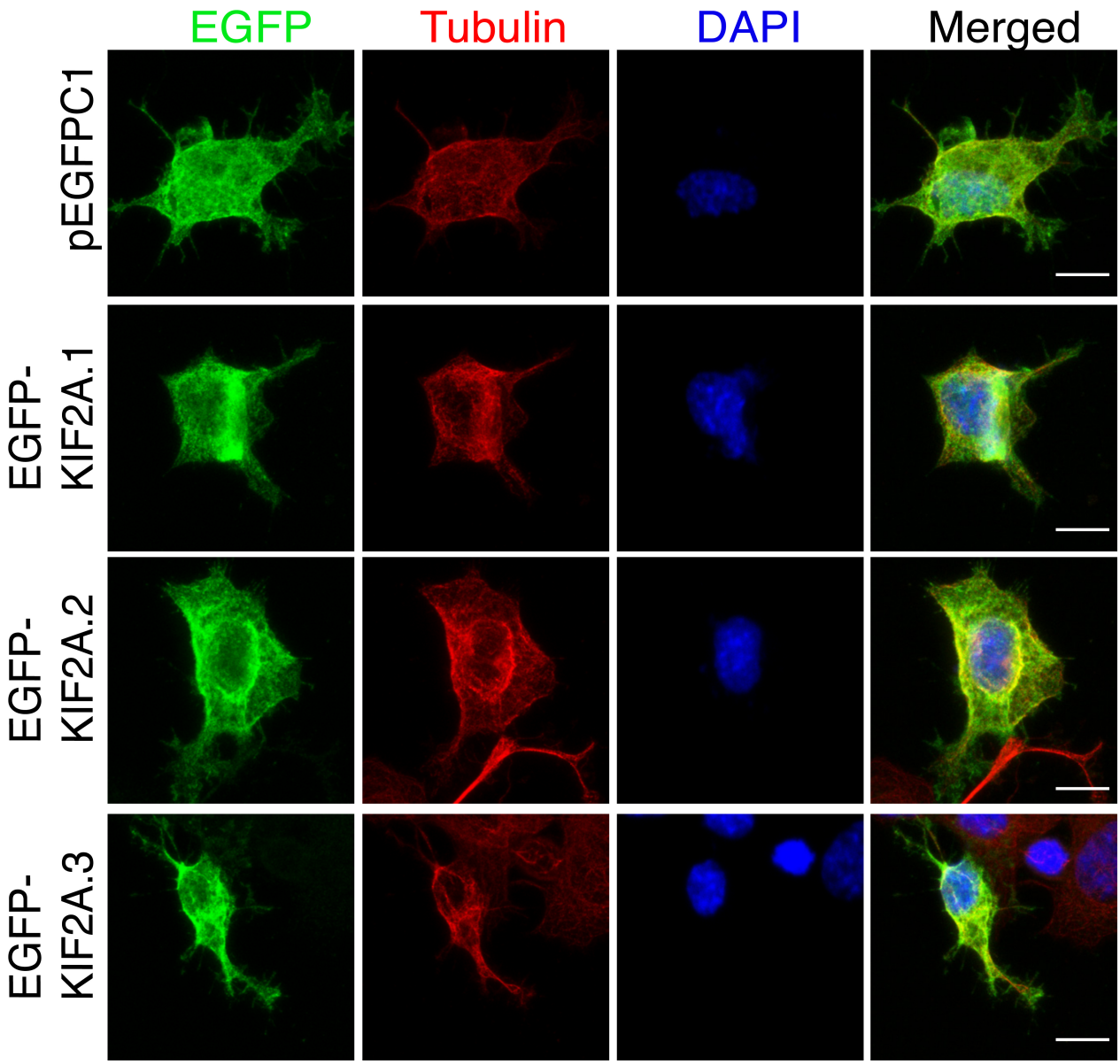

Figure S1. All KIF2A isoforms have diffused localization to cytoplasm and nucleus in Neuro2A cells. Neuro2A cells transfected with plasmids expressing pEGFPC1-tagged KIF2A isoforms (KIF2A.1, KIF2A.2 and KIF2A.3) 2 days after plating, fixed with 4% PFA 2 days after transfection and immunostained with anti-GFP (green). Anti-αTubulin visualized microtubules (red) and DAPI stained DNA. Scale bar, 10 μm.

Figure S2

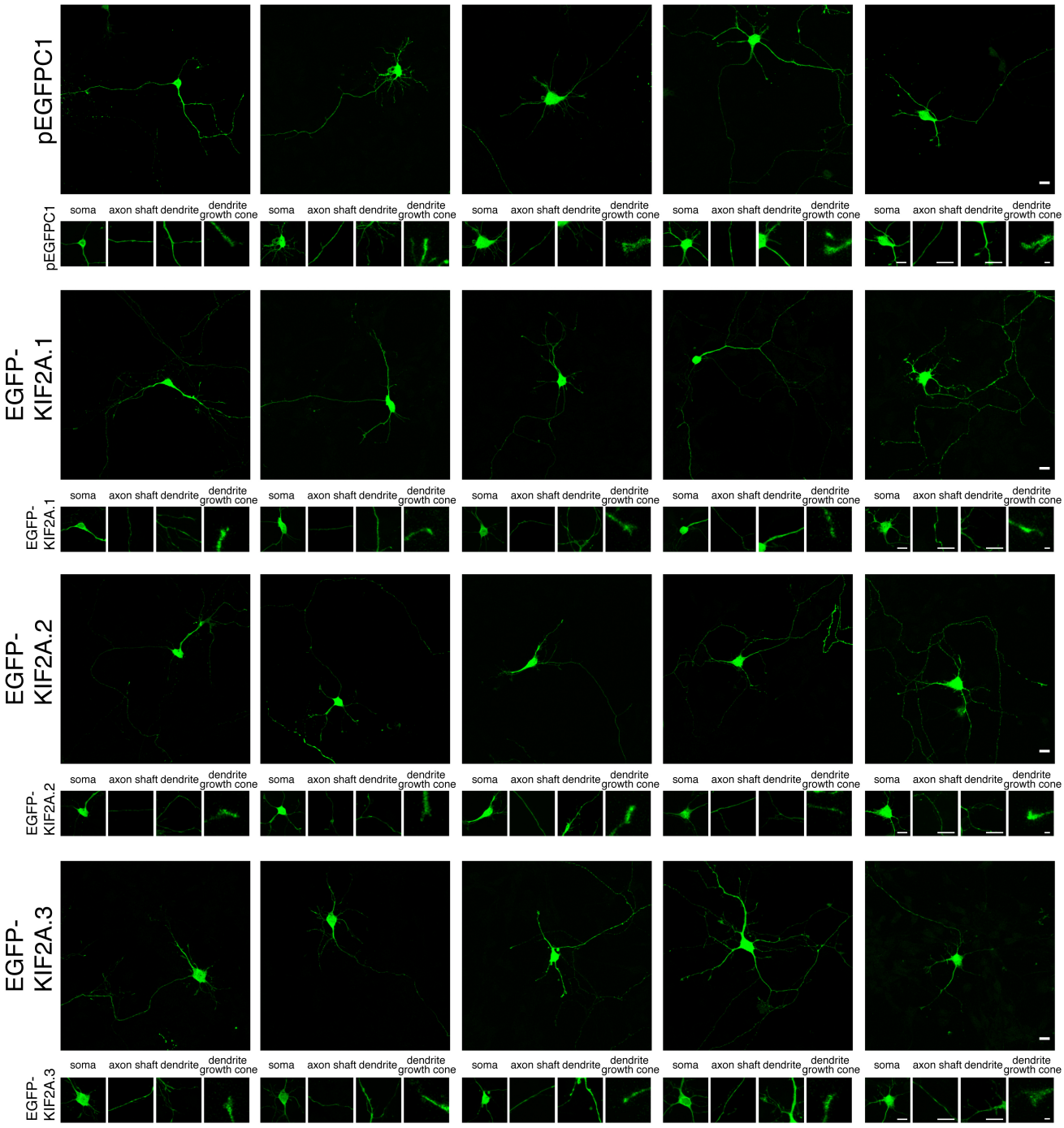

Figure S2. All KIF2A isoforms are localized to soma, axon and dendrites in primary cortical neurons. E14.5 primary cortical neurons were transfected with pEGFPC1 backbone or one of the EGFP expressing KIF2A isoforms at 2 DIV, fixed and immunostained against EGFP at 4 DIV. Digital zoom was applied to visualize localization of KIF2A isoforms in soma, axon shaft, dendrite and dendrite growth cone of each transfected neuron. 5 representative images for each condition were shown in the figure. Scale bar, 10 μm; scale bar for dendrite growth cone, 1 μm.

Figure S3

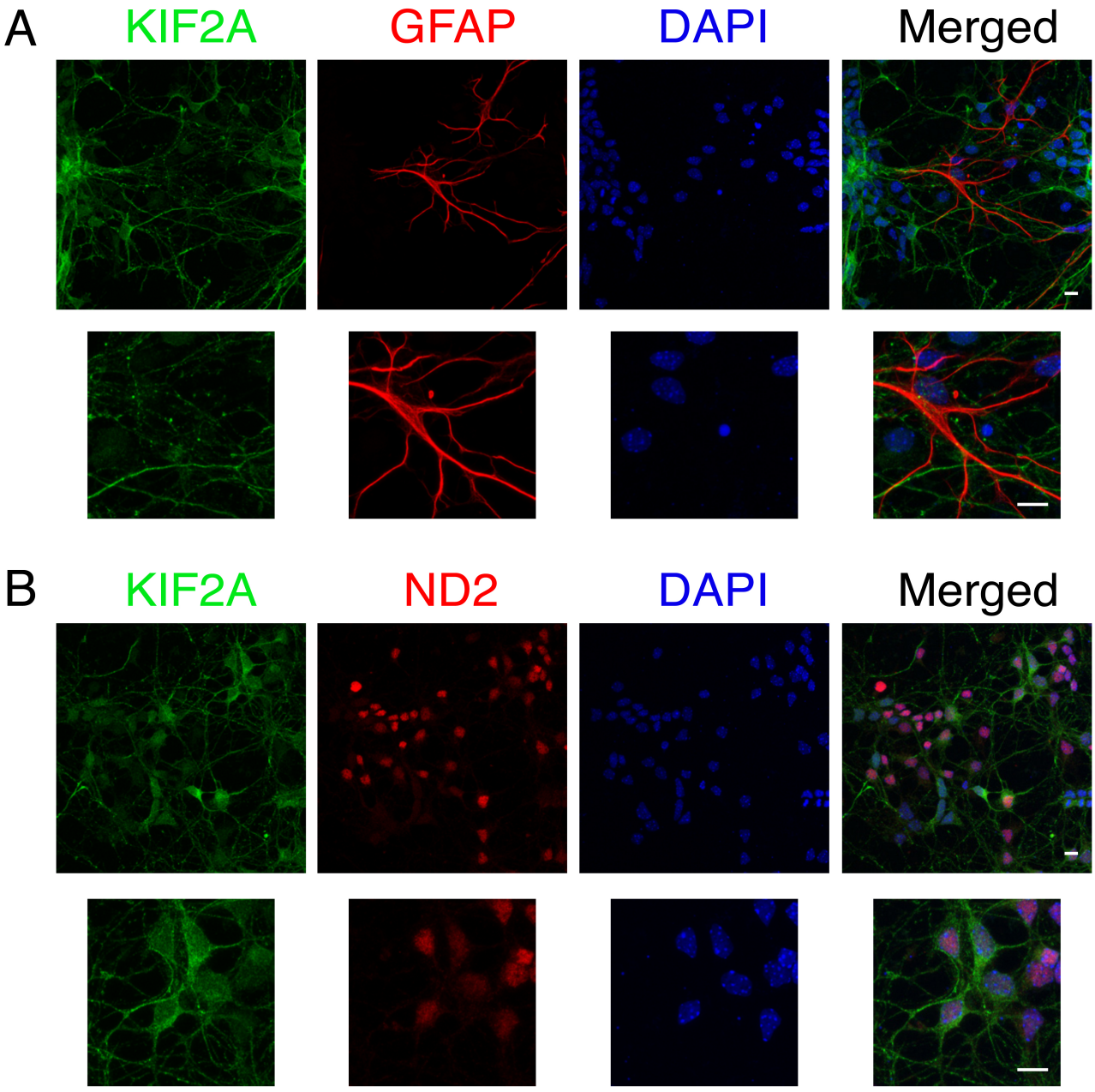

Figure S3. KIF2A is expressed predominantly by neurons but not by glia cells. A and B. E14.5 primary cortical culture was fixed at 4 DIV and stained with KIF2A (green) either anti-GFAP antibody (red) to stain glia cells (A) or anti-NEUROD2 antibody (red) to label neurons (B). Digital zoom was applied to visualize localization of KIF2A. Scale bar, 10 μm.

Figure S4

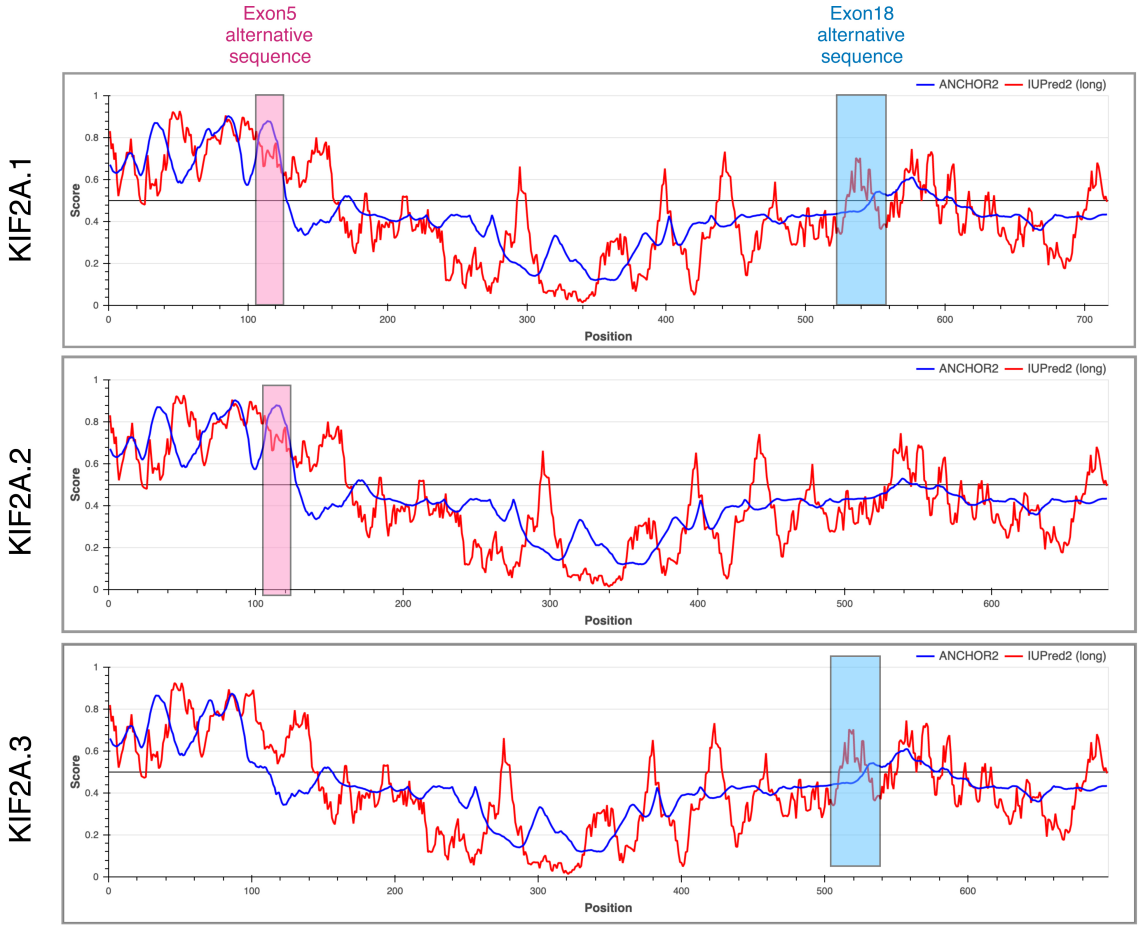

Figure S4. Measure of disorder in protein regions of individual KIF2A isoforms. A measure of protein disorder is plotted as a function of amino acid sequence of individual KIF2A isoforms. The IUPred2 and ANCHOR2 algorithms are used (Dosztányi, 2018). Alternative sequences are labeled in pink (exon5) and blue (exon18).

Figure S5

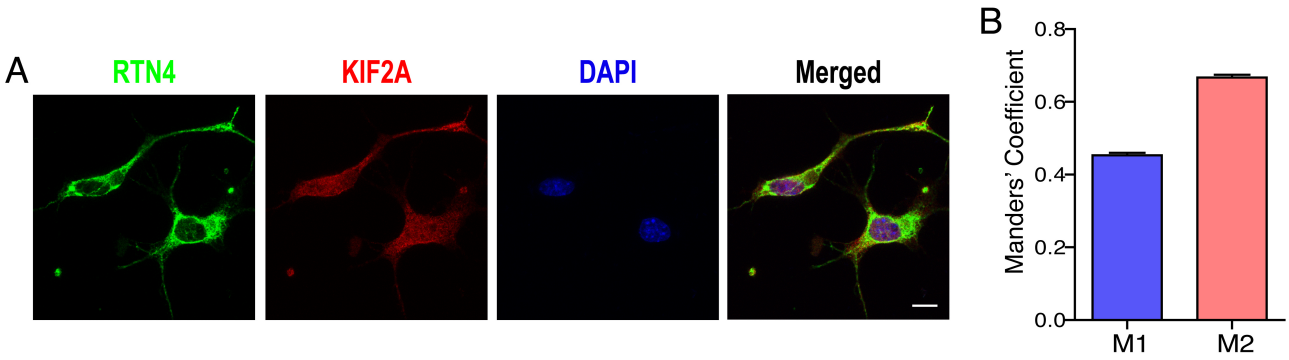

Figure S5. KIF2A and RTN4 are partially co-localized in Neuro2A cells. A. Immunofluorescence staining of RTN4 (green), KIF2A (red), DNA (blue) in Neuro2A cells. Scale bar, 10µm. **B.** Quantification of co-localization of KIF2A with RTN4A using Manders' coefficient (Dunn et al., 2011; Manders et al., 1993; Zinchuk et al., 2008). M1: Fraction of KIF2A fluorescence overlapped with RTN4 fluorescence. M2: Fraction of RNT4 fluorescence overlapped with KIF2A fluorescence. n=219, data is represented as bar graphs. Lines represent S.E.M.

Figure S6

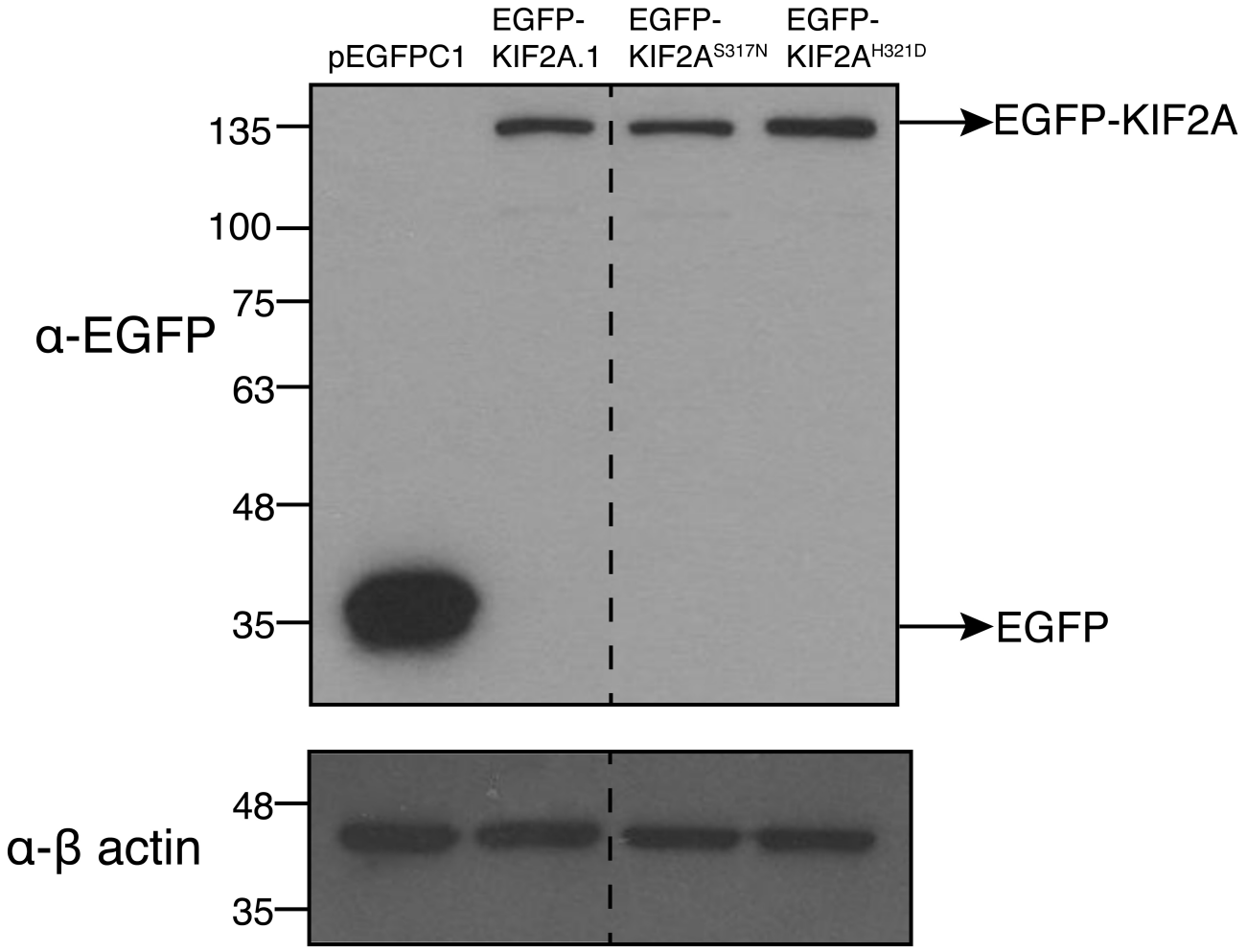

Figure S6. KIF2A mutants (*Kif2a*^{S317N} or *Kif2a*^{H321D}) expressions are similar with wild-type KIF2A and mutants do not affect protein instability. Immunoblotting with anti-EGFP demonstrating the levels of EGFP-tagged KIF2A isoforms and KIF2A mutants. B-ACTIN is used as a loading control.

Figure S7

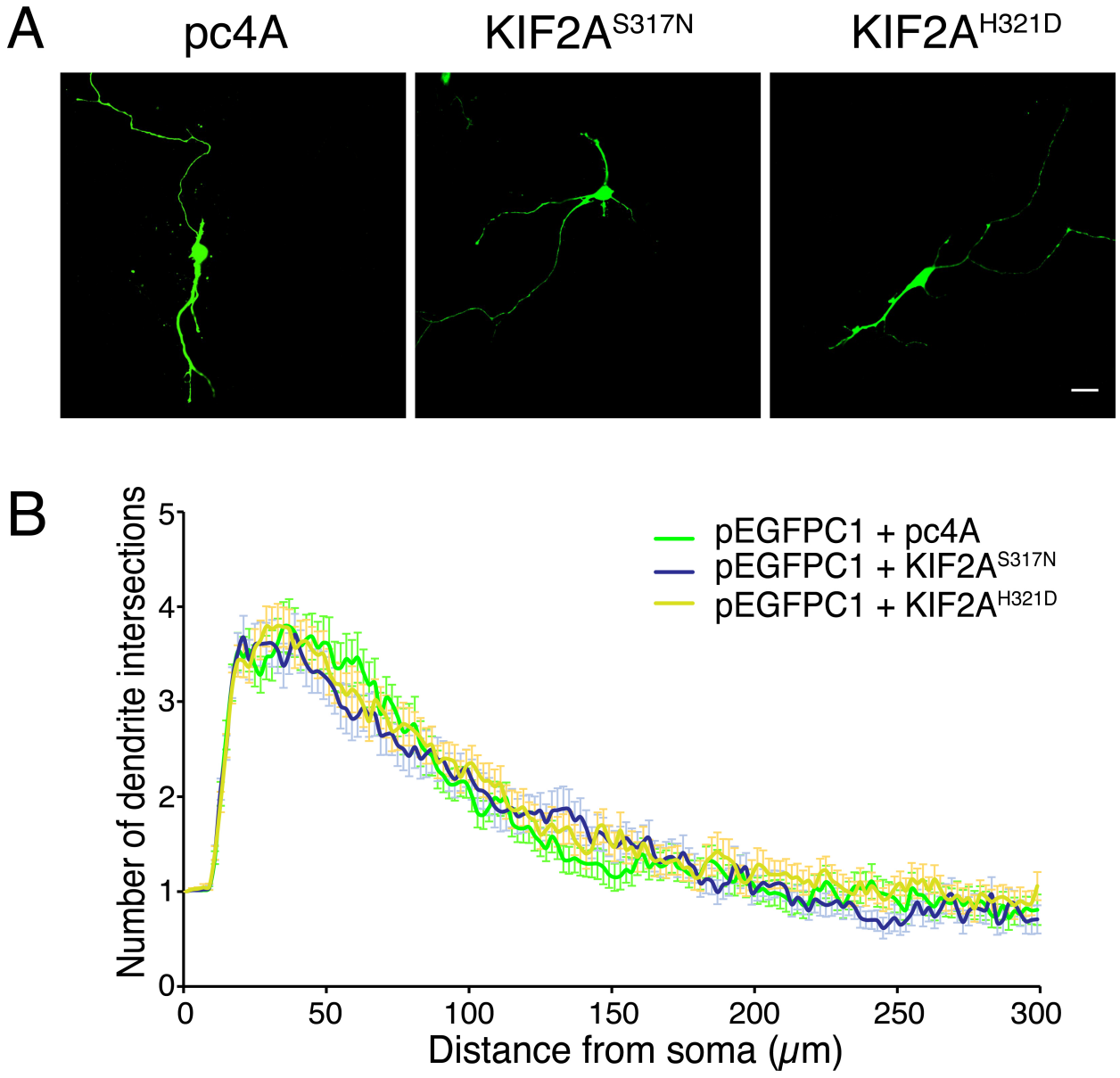

Figure S7. Expression *Kif2a*^{S317N} or *Kif2a*^{H321D} in wild-type neurons do not affect dendrite arborization. A. Representative images of E14.5 primary cortical neurons co-transfected with pEGFPC1 along with *Kif2a* mutants. Scale bar, 10 μm. **B.** Dendrite development was quantified by Sholl analysis (Ferreira et al., 2014; Schindelin et al., 2012). n=70 for each condition derived from three separate neuronal cultures. Bars represent S.E.M. Unpaired two-tailed *t* test determined the p value. $p<0.05$.

Figure S8

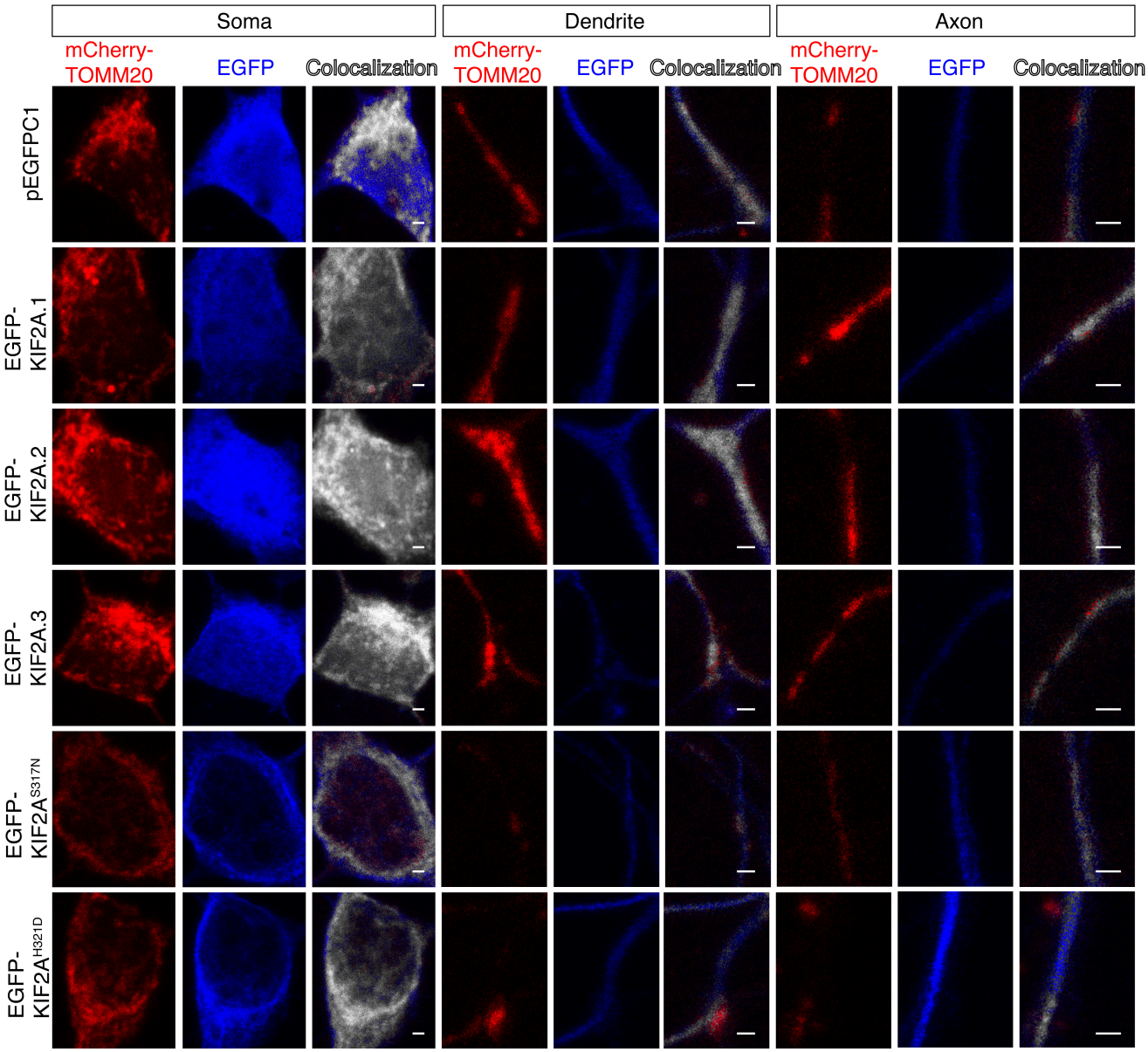

Figure S8. Co-localization of different KIF2A isoforms and *Kif2a* patient mutants with mitochondria in soma, axon and dendrites of primary cortical neurons. Magnified images of primary cortical neurons co-transfected with pEGFPC1-tagged three *Kif2a* isoforms and *Kif2a* disease mutants (*Kif2a*^{S317N} or *Kif2a*^{H321D}) along with mCherry-TOMM20-N-10. Co-localization (white) of KIF2A (EGFP, blue) with mitochondria (mCherry, red) in soma, axon and dendrite was shown in separate images by co-localization threshold tool in ImageJ. Scale bar, 1 μm.

Figure S9

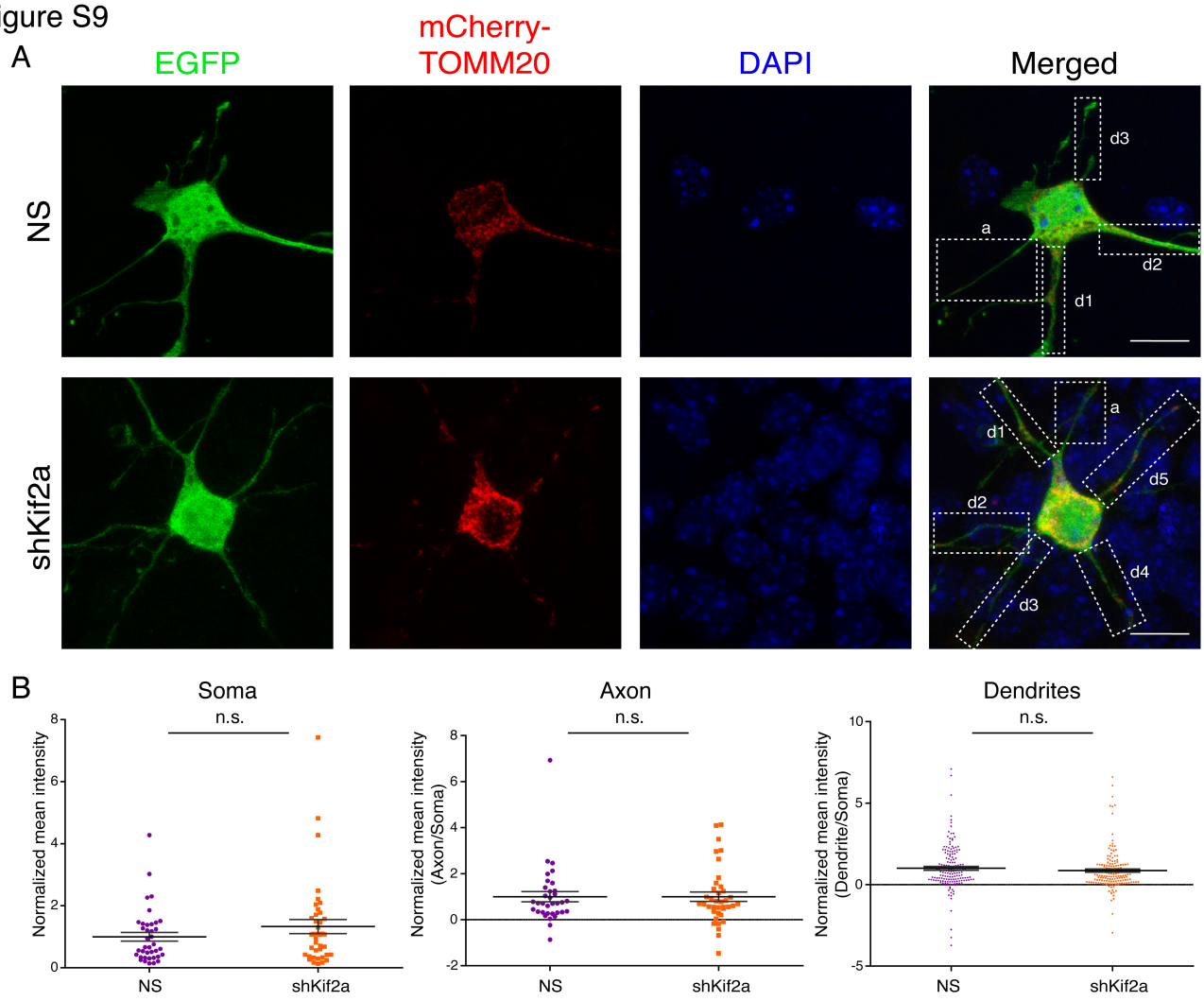

Figure S9: Silencing of endogenous *Kif2a* does not change mitochondrial localization. A. NS or shKif2a plasmids were co-transfected with mCherry-TOMM20 plasmid in E14.5 primary cortical neurons. Transfected neurons were fixed at 4 DIV and immunostained against EGFP and mitochondria were quantified based on the mCherry signal. Axon (a) and dendrites (d1-n) used for quantification were indicated with white dashed rectangles in merged channel. Scale bar, 10 µm. **B.** Quantification of images displayed in (A). Mean gray value of mCherry-TOMM20 was quantified in soma, axon and dendrites. Data of shKif2a was normalized to NS in soma. shKif2a data in axon and dendrites were normalized to soma first and then NS. n=38 for NS-mCherry-TOMM20 and n=40 for shKif2a-mCherry-TOMM20 derived from two separate neuronal cultures. Data is represented as scattered plot, lines indicate the mean number and bars represent S.E.M. Unpaired two-tailed *t* test. n.s. non-significant.

Table S1. Peptide Spectra Match Counts for BioID-mass spectrometry hits for individual KIF2A isoforms

Click here to Download Table S1

Dosztányi, Z. (2018). Prediction of protein disorder based on IUPred. *27*(1), 331-340. doi:10.1002/pro.3334

Dunn, K. W., Kamocka, M. M., & McDonald, J. H. (2011). A practical guide to evaluating colocalization in biological microscopy. *300*(4), C723-C742. doi:10.1152/ajpcell.00462.2010

Ferreira, T. A., Blackman, A. V., Oyrer, J., Jayabal, S., Chung, A. J., Watt, A. J., Sjöström, P. J., & van Meyel, D. J. (2014). Neuronal morphometry directly from bitmap images. *Nature Methods, 11*(10), 982-984. doi:10.1038/nmeth.3125

Manders, E. M. M., Verbeek, F. J., & Aten, J. A. (1993). Measurement of co-localization of objects in dual-colour confocal images. *169*(3), 375-382. doi:10.1111/j.1365-2818.1993.tb03313.x

Schindelin, J., Arganda-Carreras, I., Frise, E., Kaynig, V., Longair, M., Pietzsch, T., Preibisch, S., Rueden, C., Saalfeld, S., Schmid, B., Tinevez, J.-Y., White, D. J., Hartenstein, V., Eliceiri, K., Tomancak, P., & Cardona, A. (2012). Fiji: an open-source platform for biological-image analysis. *Nature Methods, 9*(7), 676-682. doi:10.1038/nmeth.2019

Zinchuk, V., & Zinchuk, O. (2008). Quantitative Colocalization Analysis of Confocal Fluorescence Microscopy Images. *39*(1), 4.19.11-14.19.16. doi:10.1002/0471143030.cb0419s39